Elsevier Editorial System(tm) for Composites Part B
Manuscript Draft

Corresponding Author: Prof. Wim Van Paepegem, PhD

Corresponding Author's Institution: Ghent University

First Author: Wim Van Paepegem, PhD

Order of Authors: Wim Van Paepegem, PhD; Sivakumar Palanivelu; Joris Degrieck; John Vantomme; Bruno Reymen; Dimitris Kakogiannis; Danny Van Hemelrijck; Jan Wastiels

Abstract: Crushing of composite tubes under impact loading has been studied very intensively over the last few decades. On the contrary, the energy absorption of composite tubes under blast loading is much less studied, and very limited public literature is available. This paper presents the experimental testing of a sacrificial cladding structure, composed of glass/polyester tubes, under blast loading. The composite tubes show stable and progressive crushing and considerably lower the peak force transferred to the non-sacrifical structure.

BLAST PERFORMANCE OF A SACRIFICAL CLADDING WITH COMPOSITE TUBES FOR PROTECTION OF CIVIL ENGINEERING STRUCTURES

W. Van Paepegem[1*], S. Palanivelu[1], J. Degrieck[1], J. Vantomme[2], B. Reymen[2], D. Kakogiannis[2], D. Van Hemelrijck[3], J. Wastiels[3]

[1] *Department of Materials Science and Engineering, Ghent University, Technologiepark-Zwijnaarde 903, 9052 Zwijnaarde, Belgium*
[2] *Royal Military Academy, Civil and Materials Engineering Department, Building G, Level 0, 8 Av. Hobbema B-1000, Brussels, Belgium*
[3] *Department of Mechanics of Materials and Constructions, Vrije Universiteit Brussel, Pleinlaan 2 B-1050 Brussels, Belgium*

*Wim.VanPaepegem@UGent.be

Abstract

Crushing of composite tubes under impact loading has been studied very intensively over the last few decades. On the contrary, the energy absorption of composite tubes under blast loading is much less studied, and very limited public literature is available. This paper presents the experimental testing of a sacrificial cladding structure, composed of glass/polyester tubes, under blast loading. The composite tubes show stable and progressive crushing and the peak force transferred to the non-sacrifical structure is compared for different configurations of the composite tubes. The results also show that the diffraction of the pressure wave and the skin panel that distributes the blast pressure are critical issues in the set-up of the experiments.

Keywords:

A Polymer-matrix composites

B Impact behaviour

C Numerical analysis

D Mechanical testing

1 Introduction

When civil engineering structures are subjected to blast loading, the failure of the critical load bearing members such as beams, pillars, columns etc., and its debris can cause major human casualties. Hence a preventive solution is needed to safeguard those civil engineering structures. Out of many proposed solutions, the concept of sacrificial claddings has attracted a lot of attention [1-6] in terms of its functionality and its predictable behaviour. Any sacrificial cladding structure can have two layers (an inner core and outer skin panels). The function of the skin panel is to distribute the blast pressure more evenly to the inner core which deforms progressively and absorbs most of the energy from the blast load, so that the main load bearing members of the civil engineering structures will be safeguarded.

In case of impulsive blast loading on civil engineering structures and sacrifical cladding structures, the positive duration of the blast load will be much shorter than the natural period of the structure. In order to protect civil engineering structures from such a blast load, the proposed sacrificial cladding structure should be mounted or assembled in front of those structures. During a blast loading the sacrificial cladding structure will receive a high load (p_0) - short duration impulse (Figure 1). The function of the sacrificial cladding structure as a whole is to change the force-time distribution from a high load - short duration impulse to a low load - long duration impulse (Figure 1). To avoid permanent damage in the main structure (non-sacrificial structure), the failure load of the sacrificial cladding structure (F_{max}) should be kept well below the minimum elastic capacity of the non-sacrificial cladding structure. By doing so, the transferred peak force to the non-sacrificial structure can be minimised [7]. The mechanism by which a sacrificial cladding structure does this, is absorbing energy through elastic, plastic or brittle deformations. During this process the conservation of (linear)

momentum should be satisfied. Furthermore, the blast loads typically produce very high strain rates. The strain rate and the corresponding strain hardening alter the dynamic mechanical properties of the target structures (sacrificial cladding structure). Hence, these factors should be thoroughly studied and taken into account while deploying a material for the inner core of a sacrificial cladding structure.

This contribution focuses on a sacrificial cladding structure with the core consisting of an array of composite tubes which should be responsible for the major energy absorption from the blast. Over the past years, a lot of research has been done on crushing of tubes for energy absorption [8-20]. The authors themselves have studied the energy absorption of a single composite tube under axial impact and air blast loading [21-26]. Those models for crushing have been thoroughly validated by small-scale drop weight tests and blast tests in a bunker. The purpose of the research presented here, is to validate the proof-of-concept with larger-scale air blast tests on a representative sacrificial cladding structure, composed of pultruded glass/polyester composite tubes as core material and sandwich composite skin plates.

2. Behaviour of the pultruded glass/polyester tubes under varying strain rate

In a first step, the strain rate sensitivity of the pultruded glass/polyester tubes is investigated. This step is very important, because many insights from quasi-static and impact loading can be transferred directly to the blast loading tests, if the strain rate sensitivity is limited.

The material, architecture and dimensional parameters of the composite tubes for the blast loading are the same as for the quasi-static and impact testing, previously conducted by the authors [21-26]. The tubes consist of pultruded unidirectional glass fibres in a polyester matrix. The cross-section is circular or square and wall thicknesses are chosen such to assure stable and progressive crushing. The effect of filling the hollow tubes with foam, has been studied in quasi-static and impact loading [23] and shows that foam filling is only beneficial if

3

the density of the foam is sufficiently low. If the foam density is too high, the inward bending of the petals is prevented and the progressive delamination is suppressed. This results in a smaller specific energy absorption (SEA), compared to hollow tubes.

2.1. Consistency of deformation patterns

In quasi-static and impact loading, it was observed that the inner and outer petals were formed due to the circumferential delamination and, consequently, axial cracks were formed parallel to the axis of the tube. The uniform geometry of the circular tube facilitated to form more axial cracks and, thus, more petals were formed. The major amount of impact energy was absorbed due to the increasing number of longitudinal cracks and subsequent bending of the laminae [21].

To conduct close-range free air blast tests on a single composite tube, a special laboratory test set-up was designed and manufactured (Figure 2). The spherical explosive (typically 20-50 g) is hanging above the test set-up. After detonation, a spherical shock wave propagates towards the skin plate, that transfers the blast pressure to a single composite tube underneath it. That composite tube is progressively crushed and a side cover tube prevents the blast pressure from acting sideways on the composite tube during deformation. Different parameters have been varied in the experiments, such as spherical explosive (C4) mass, stand-off distance, area of skin plate and mass of the skin plate. The incident angle for all tests was zero.

During the air blast tests, the following parameters were measured:
- the incident pressure (with a blast pencil)
- the reflected pressure at the surface of the skin plate (with a pressure sensor)

4

- the accelerations of the skin plate (with an accelerometer), and by integration, the velocity and displacement of the skin plate,

- the transferred load to the "non-scacrificial structure" (by a load cell below the composite tube),

- digital high speed imaging of the blast event.

The deformation patterns of the circular cross sectional composite tubes are shown in Figure 3. It can be noticed that the crushing failure mechanisms of these tubes are the same as for the quasi-static testing results.

Further, it has been investigated if the same conclusion applies for different thickness/diameter ratios. To that purpose, thicker commercially available pultruded glass polyester composite tubes (M/s Exel composites, Belgium) have been tested. The deformation patterns of these tubes under blast loading are presented in Figure 4 and are again in accordance with static deformation patterns.

Furthermore, the same finding was also validated for contact blast loading using a suspended pendulum test set-up which was developed in collaboration with Prof. Gerald Nurick from University of Cape town, South Africa (Figure 5(a)) [27]. Tests have been conducted on this pendulum set-up with different sizes of cylindrical charge masses and with different striker masses. As an example, the deformation patterns of the tubes subjected to contact blast loading are given in Figure 5(b). The failure mechanism and the patterns of these tubes are the same when compared to quasi-static experimental results. Hence, it can be concluded that the failure mechanisms and the failure patterns of these tubes (unidirectional glass polyester composite tubes) seems to remain identical irrespective of the strain rate.

2.2. Strain rate insensitivity

The pultruded composite tubes show strain rate insensitivity over the complete range of loading from quasi-static testing till free air blast loading.

Figure 6 shows the comparison of the force-deformation curves of composite tubes with triggering type 1 (45° chamfering) and triggering type 2 (tulip triggering) for quasi-static, impact and blast loading conditions. Figure 6(a) shows the average force-deformation curves (from 4 tests of each type) of circular cross sectional composite tubes with triggering type 1. The quasi-static tests were performed with a cross head displacement of 10 mm/min; impact tests were performed for an initial impact velocity of 6.0 m/s with an impactor mass of 7.6 kg; and the free air blast tests were performed for 40g of C4 with stand-off distance of 30 cm. It can be noticed that the average peak crush load of these cases is very close to each other (deviation of less than 10 % of the peak crush loads). A similar result was also observed for triggering type 2 (refer Figure 6(b)). Based on the results of the experiments presented hereto, it can be concluded that for uni-directional fibre orientation the effect of strain-rate on the peak crush load is negligible. Similar results have also been reported for glass polyester pultruded composite tubes in ref [28].

Due to the same deformation patterns in all loading conditions (quasi-static, impact and blast) and the absence of strain-rate effects on the peak crush load, the influence of the triggering mechanism on the force-deformation curves remains the same when compared to quasi-static tests (Figure 6(a) and 6(b)). Unlike for the quasi-static tests and impact tests, the crush load of the tubes for blast load decreased after the peak load. This was due to the short duration of the loading and a lower skin plate mass (compared with quasi-static and impact loading) resulting in a lower deformation length.

2.3. Simulation of the experimental set-up

In order to understand the efficiency of the composite tubes for energy absorption under blast loading, the impulse delivered to the top face of the skin plate (reflected impulse) and the corresponding transferred impulse at the bottom of the composite tube to the non-sacrificial member (integration of measured force-time history at the bottom of the composite tube) were compared. Approximately 30 % difference between the reflected impulse and the transferred impulse was observed in all cases, and hence, the linear momentum was not conserved for any of the cases. This result is unexpected, because a sacrificial cladding structure cannot prevent the impulse of the blast being transferred onto the structure upon which it is mounted, rather it changes the force-time distribution from a high load, short duration impulse to a low load, long duration impulse and thereby avoiding or reducing the damage to the nonsacrificial structure upon which it is mounted.

In order to understand the large difference between reflected and transferred impulse, the whole experimental set-up was also modelled in the finite element code Autodyn. In order to reduce the computational time the blast simulation for the discussed experimental set-up was done in two stages. The first stage is the analysis of the detonation of the C4 explosive and propagation of the pressure waves. In Autodyn v12.1 this analysis can be done using a 2D approach.

The detonation of the C4 explosive was modelled with a wedge (Figure 7). Accordingly 1000 grids (elements) were chosen along the radial axis in the air medium. The air and C4 were modelled using *multi-material Euler formulation*. The initiation, detonation and the expansion of C4 was modelled using the *Jones-Wilkins-Lee* (JWL) Equation of state (EOS).

The spherical charge of 20g C4 was modelled with an equivalent radius of 14 mm in the 2D model. Similarly, the wedge area filled with ambient air was modelled using the ideal gas equation.

In order to compare the incident blast parameters, the results from the Hydrocodes calculation was compared with *ConWep* data for the same input parameters (20 g C4 and 30 cm stand-off distance). Figure 8 shows a comparison of the incident blast parameters (arrival time, peak incident pressure and the positive phase duration) from Autodyn, *ConWep* and experimentally measured data. For the simplification only the positive phase of the pressure-time history is considered.

The magnitude of peak incident overpressure from the experimental measurement and the calculated value from Autodyn were very close to the *ConWep* predicted data (923 kPa, 920 kPa and 898.7 kPa from the experiment, Autodyn and *ConWep* respectively). Furthermore, there was a good correlation observed for arrival time and positive phase duration between the experimentally measured data (0.121 ms and 0.378 ms respectively) and Autodyn simulated values (0.126 ms and 0.37 ms respectively). However, the predicted time of arrival and the positive phase duration from ConWep showed longer durations (0.162 ms and 0.6941 ms for arrival time and positive duration of the blast respectively).

The second part deals with the propagation of blast pressure in a 3D computational model using 2D data. The remapping option of Autodyn provides this feature.

The air was modelled as a rectilinear box with Eulerian grid. The boundary of the air model was chosen to have adequate air space in all directions from the centre of detonation. The dimensional details and the 3D computational modelling of the experimental set-up are shown in Figure 9.

On the rectilinear air flow domain, the "flow-out" boundary condition was assigned to all boundary planes of the 3D domain except the base plane, which represented the ground surface. This boundary condition is needed to simulate the reflection of pressure waves from the ground surface. The interaction of blast pressure waves with the aluminium skin plate and

the side tube was defined by a fully coupled feature available in Autodyn v12.1. The fully coupled algorithm allows the Lagrange and the Euler-FCT (Flux Corrected Transport) formulation to be coupled in a single problem. With help of this approach a high order solution is computed wherever possible in the flow field. This coupled algorithm automatically detects the interfacing faces of the aluminium skin plate, the side cover tube and the rigid support. These interfacing faces act as a physical constraint to the fluid domain. Consequently, the resultant shock from the pressure waves on the aluminium skin plate will be transferred to the test specimen.

The magnitude of the reflected pressure wave was calculated at the air grid which was closer to the top and bottom faces of the skin plates (1 μm away from the faces). In order to study the effect of the grid size on the blast parameters, a mesh sensitivity study was conducted for the air model with the aluminium skin plate (ϕ 200 mm; 1.0 kg) with the following grid sizes : 0.25 mm, 0.5 mm, 1 mm, 5mm, 10 mm and 15 mm. Only for the smallest element sizes (0.25 mm and 0.5 mm) the magnitude of the peak reflected pressures (4849 kPa and 4745 kPa respectively) was very close to the ConWep value (4755 kPa). An element size of 0.25 mm was used for all the analyses.

The clearing of reflected pressure waves and the subsequent diffraction phenomenon can be explained by investigating the propagation and interaction of blast pressure waves with respect to time. As an example, the 30 cm stand-off distance case is discussed here. Figure 10 shows the interaction of the pressure waves (at the mid-plane representing X = 0 and Z = 0) with the top and bottom faces of the aluminium skin plate. These figures show a chronological event of interaction and diffraction of the pressure waves around the edges of the aluminium skin plate. As we have mentioned earlier the remapping of the 2D blast wave was fed into the 3D computational model. After remapping, the analysis was started when the pressure reached 0.25 mm above the top face of the skin plate (this corresponds to time t = 0

ms). The magnitude of the pressure wave increased suddenly when the incident pressure was obstructed by the top face of the skin plate. Due to the spherical wave front, a higher magnitude was observed at the centre of the top face of the skin plate. This event started after approximately 0.8 μs at the centre of the top face of the plate and it lasted for approximately 1.9 μs. After that the amplitude reduced exponentially. During this period a significant amount of pressure waves (especially the pressure wave at the periphery of the top face of the skin plate) diffracted around the top edge of the skin plate (clearing phenomenon). Due to this clearing the magnitude of the reflected pressure wave was reduced significantly in a short time.

The later time increments of the analysis showed the interaction of ground reflected pressure with the skin plate. As an example, the numerical evidence of the interaction of pressure waves from the ground reflection for 30 cm stand-off distance is shown in Figure 11.

The impulse from the diffraction and ground reflection was opposite to the direction of the reflected impulse at the top face of the skin plate. Therefore, the resultant impulse imparted to the top skin plate and the corresponding transferred impulse (I_{trans}) to the solid copper tube was equal to the difference between the reflected impulse and the combined impulse from the diffraction and ground reflection ($I_{resultant} = I_{ref} - I_{diffraction} - I_{ground\ reflection}$). The calculated combined impulse from diffraction and ground reflection at the bottom face of the skin plate was approximately 31% and 29.4% of the total reflected impulse at the top face of the aluminium skin plate ($\phi\,250$ mm; 1.0 kg) for 30 cm and 15 cm stand-off distance respectively. Now, these values (31% and 29.4%) can be compared with the average difference in impulse ($\Delta I = I_{refl} - I_{trans}$) observed during the experimental testing. The average difference in the experimental impulse varied from a minimum of 28% to a maximum of 33 %. From the results of the above analyses it can be concluded that approximately 30% of the total impulse was lost due to the diffraction and ground reflection phenomena.

The outcome of the numerical simulations was also confirmed by the high speed images in Figure 12, which show a very quick clearing of the pressure waves around the edges of the top skin plate. Based on these insights, the transferred impulse to the specimen had to be corrected for diffraction and ground reflection.

These findings are very important for the correct interpretation of the efficiency of the sacrificial cladding in the larger-scale blast tests (see next section), because apparent losses of reflected impulse can strongly bias the conclusions about efficiency of the proposed sacrificial cladding solution.

3 Materials and methods for large-scale blast tests

The global view of the experimental test set-up is shown in Figure 13. The glass/polyester tubes were mounted on a (rear) sandwich composite skin plate behind which three dynamic force sensors were connected to a concrete wall to measure the transferred impulse to the concrete structure (which has to be protected from the blast). The locations of the force sensors were equidistant from the centre and the angle between these sensors was 120°. Another skin plate was assembled on the front side of the glass/polyester tubes (test specimens). The diameter of both front and rear sandwich skin plates was ϕ 0.96 m, in order to have a small clearance with the concrete pipe (ϕ 1.0 m) for easy assembly. The front skin panel was instrumented with three pressure sensors and two accelerometers to measure the reflected pressure and the acceleration of the skin plate respectively (Figure 13). The mass of the front skin panel was approximately 7.15 kg including all sensors. The crushing face of the front sandwich skin panel was in-line with the end of the concrete tube which was close to the concrete wall. The C4 charge was placed at the other end of the concrete pipe (stand-off

distance was 4.2 m). Blast experiments have been conducted for two configurations of the composite tubes (25 and 37 tubes) with different charge masses (100g and 150g of C4).

To hold the composite tubes in horizontal position on the rear skin panel during blast loading, soft foam holders were adhesively bonded on the rear skin panel (Figure 14(a-b)). The stiffness of this foam was very less; hence, the resistance provided by the foam during the blast loading can be neglected. Two high speed cameras were used to capture the crushing behaviour of the glass/polyester tubes during the blast loading. Their view was similar to Figure 14b.

All the skin plates used for the large-scale blast tests were manufactured by M/s Acrosoma, Belgium. The sandwich composite skin plates were made of three materials (Figure 15). The outer face sheets (top and bottom) were made of bi-axially balanced glass fibre with polyester resin; the core structure was made of divinycell P foam. The outer face sheets were stitched together straight through the foam with aramid fibres. This prevented the delamination between the face sheets and the core structure.

Before conducting blast tests on the sacrificial cladding, the minimum length of the concrete sewage pipe to provide a perfectly plane shock wave should be known. Hence, coupled numerical simulations have been conducted for different charge masses and with different lengths of concrete sewage pipes to identify the length which was required to have a perfectly plane shock wave. The commercially available code Autodyn v12.1 was used for this purpose. To reduce the computation time the concrete pipes and the front skin panel were modelled with a rigid material. The length of a single concrete pipe was 2.1 m. Hence, the discrete length was dictated by the length of one concrete tube. The air and C4 were modelled

using the *multi-material Euler formulation*. The initiation, detonation and the expansion of C4 were modelled using the *Jones-Wilkins-Lee* (JWL) Equation of state (EOS). Similarly, the volume filled inside the concrete pipes with ambient air was modelled using the ideal gas equation of state. Different lengths and charge masses have been considered to achieve a perfectly plane shock wave at the other end of the concrete pipe. A fixed boundary condition was used for the skin panel to calculate the reflected pressure time histories. As an example, the simulated propagation of the pressure wave inside the concrete sewage pipes for 150g C4 with 4.2 m stand-off distance is shown in Figure 16. It can be noticed from Figure 16 that a perfectly plane shock wave is formed at the other end of the tube.

Also, the comparison of the experimentally measured and numerically calculated (Autodyn simulation) reflected pressure-time histories showed a very good correlation for peak reflected pressure and the positive duration of the blast (Figure 17). It was essential to account for the clearing of the pressure waves at the end of the concrete tube, due to the small mismatch in diameter between the sandwich plates and the concrete pipe (ϕ 0.96 m vs. ϕ 1.0 m). Without taking into account this clearance, the reflected impulse was overestimated by 33 % ! As shown for the small-scale blast tests, this proves again the importance of clearing and diffraction of the incident pressure waves.

The consolidated reflected blast parameters (peak reflected pressure, positive duration and the corresponding reflected impulse) from the Autodyn simulations for the case of 150 g C4 are presented in Table 1.

All pultruded small-scale composite tubes used for the large-scale blast testing were reinforced with 18 streams of 4800 tex glass roving (P192 type from M/s OCV). The volume

fraction of the fibre was approximately 50%. The POLYLITE® 413-010 resin (un-accelerated, non-thixotropic, medium reactive orthophthalic polyester resin) was used to manufacture the composite tubes. In order to achieve a uniform and progressive deformation pattern the thickness/diameter ratio of 0.045 was chosen. The dimensional and material details of the composite tubes are given in Table 2. The composite tubes have been cut for 100 mm length and filled with low-density foam, to achieve stable crushing with this very low wall thickness of 1 mm. To induce the failure at lower crushing force, the 45° chamfering (triggering mechanism) was introduced at one end of the composite tubes. Preliminary quasi-static and impact investigations have been performed to check the progressive crushing deformation patterns of these tubes (Figure 18).

4. Experimental results

The global deformation patterns of the composite tubes with 150 g of C4 are shown in Figure 19(a) and (b) for configuration 1 (25 tubes) and 2 (37 tubes) respectively. As an example, the final deformation patterns after the blast experiment of two composite tubes for each configuration are shown in Figure 20(a-d). It can be noticed from these figures that the deformation patterns of the composite tubes are consistent; and all typical failure modes are clearly evident (axial cracking, fibre failure, delamination, bending of petals). The average deformation length for configuration 1 (25 tubes) was higher (55.7 mm) than for configuration 2 (37 tubes) (33.7 mm).

Similar to the quasi-static and impact tests, the presence of the polyurethane foam prevented the axial splitting of the tube wall. In addition to that, the low density of the polyurethane

14

foam did not affect the continuous delamination and subsequent fibre fracturing failure modes which are very good irreversible energy dissipation mechanisms.

The experimentally measured load time histories for three different cases are shown in Figure 21(a-c) for 100 g of C4 with 25 composite tubes, 150 g of C4 with 25 composite tubes and 150 g of C4 with 37 composite tubes respectively.

The corresponding consolidated average parameters for these cases are given in Table 3. The reference test (last row in Table 3) has been considered as the one, where the front skin panel and the rear skin panel are placed side by side, without any tubes in between. Of course, this configuration with the two sandwich panels will also absorb energy, but the effect of the tubes can be isolated in this way.

For the case with 100 g of C4, the data from one test could not be measured due to some problems. Hence, for this case the data from only one test is presented. From Figure 21(a-c) and Table 3, it can be noticed that irrespective of the charge mass the peak crush load for configuration 1 (25 composite tubes) remained the same. The peak crush loads for 100 g of C4 and 150 g of C4 were 87.75 kN (from one test) and 86 kN (from two tests) respectively. For configuration 2, the average peak crush load of 103.1 kN was noticed due to a higher number of composite tubes. Similarly, the positive duration was extended approximately to 8.2 ms, 9.5 ms and 9.2 ms for 100 g C4 with 25 composite tubes, 150 g C4 with 25 composite tubes and 150 g C4 with 37 composite tubes respectively.

There was a clear difference observed between the reflected impulse and the transferred impulse. The configuration 1 with 100 g and 150 g of C4 showed higher transferred impulses than for configuration 2 with 150 g of C4. The reason was that the lower number of composite tubes (for configuration 1) provided a lower resistance to the front skin panel and as a consequence a corresponding lower reaction load to the rear skin panel. However, for the case with 37 composite tubes (configuration 2) the reaction load to the rear skin panel was larger due to the larger number of composite tubes. Due to the larger reaction load and an inadequate bending stiffness, the rear skin panel was subjected to global bending during the initial stages of crushing. The bending of the rear skin panel (pin-supported on the three load cell sensors) was so high that its edge touched the concrete wall. Therefore, a significant load was directly transferred to the concrete wall and bypassed the load cell sensors. Therefore, the transferred impulse (integrated load time histories) measured from the load cells was lower for configuration 2 compared to configuration 1.

This is clearly illustrated by the sequence of high speed images in Figure 22. The edge of the shock tube is at the left, the concrete wall is at the right. The first image shows the "flash" when the C4 explosive detonates at the other side of the shock tube. In the second picture, the clearing of the pressure waves through the radial gap between the inner diameter of the shock tube and the front skin panel can be seen clearly. The third picture shows the progressive crushing. The fourth picture shows the severe bending of the front and rear skin panel in the top of the picture. The fifth picture shows the negative phase of the blast, where the front skin panel is "sucked" back into the shock tube.

The duration of the negative phase in all experiments appeared to be very long. In almost all experiments, the front skin plate could be found back at the entrance of the shock tube after the test. The large underpressure made the front skin panel travel backwards through the

complete length of the 4.2 m long shock tube. At the same time, it confirmed the very uniform

progressive crushing of the array of composite tubes, because the radial clearance was very

small (20 mm), and yet, the front skin panel moved backwards concentrically into the shock

tube.

Finally, in order to validate the observed bending behaviour of the skin panels, a numerical

model was built. The authors developed detailed finite element models in the past for crushing

of circular and square tubes [25,26], but those are computationally too expensive to apply to a

set of 25 or 37 composite tubes. Therefore the composite tubes were modelled in the finite

element simulation as equivalent energy absorbing tubes with the correct force-displacement

curve, but without incorporating all the observed failure modes (delamination, fibre fracture,

laminae bending). On the other hand, the sandwich composite skin panels were modelled in

detail, in order to validate the observed behaviour.

The numerical modelling of the sandwich composite skin panel was done as per the assembly

sequence in Figure 15. The top and bottom composite skin faces were modelled with shell

elements. The meshed shell elements were located at the centre of the thickness of each

composite laminate. The strength model of the divinycell P foam was represented by means of

the compressive crush characteristics (refer Figure 23).

It was assumed that the top and bottom composite plates and divinycell P foam were tied

together due to the stitch with aramid fibres. This was also supported by the experimental

observations. Accordingly a tied connection was established at the interfaces of all these parts.

Similar to the experimental conditions, the dynamic load cells were modelled as rigid bodies

to measure the load time histories. The concrete wall was modelled as a rigid body;

subsequently a reference point was introduced to capture the total impulse transferred to the

concrete wall. An equivalent triangular time dependent pressure was applied to the top face of the top skin panel.

The initial time increments showed that the front skin panel underwent a significant compression. Due to the applied blast pressure on the front face of the front skin panel the foam core reached its densification regime and it stayed in that regime until the test specimens reached their maximum deformation length. There was no significant compression observed in the rear skin panel until the foam core of the front skin panel reached its densification regime. The compression of the foam core of the rear skin panel started when the front skin panel reached its densification regime. However, the compression of the foam core was rather uniform through the entire surface of both front and rear skin panel. When the composite tubes reached their maximum deformation length, the entire rear skin panel started to bend. Subsequently, the rear skin panel came into contact with the concrete wall. A similar evidence was also noticed from the experimental results. Furthermore, a local compression of the skin plates (both front and rear) was significant at the individual mounting locations of the composite tubes, where the local reaction forces were transferred to the skin plate.

As an example, the fibre and matrix failure modes of the bottom face of the rear skin panel and bottom face of the front skin panel are shown in Figure 24(a-d) and Figure 25(a-b). It can be noticed that the tensile failure of fibres and matrix was significant. The shell elements at the load cell mounting locations showed a complete failure. The same evidence was observed from the experimental results; the foam core at the mounting locations delaminated from the face plates. Similarly, for the front skin panel, high chances of failure can be expected for the areas which were in contact with the composite tubes. Finally, the stress distribution of the foam core (divinycell P foam) of the rear skin panel is shown in Figure 26.

5 Conclusions

The small-scale blast tests on pultruded composite tubes lead to the following conclusions:

- in addition to several parameters such as the thickness/diameter ratio, linear density and triggering mechanisms, the uniform distribution of the wall thickness plays a significant role to achieve progressive deformation patterns in thin-walled composite tubes. For the chosen composite tubes (pultruded glass polyester composite tubes with wall thickness of 1.0 mm) the catastrophic failure modes were avoided by filling the tubes with a low-density polyurethane foam.

- the conducted axial quasi-static, impact and blast experiments have shown that the deformation patterns of these composite tubes remain the same. The typical brittle failure modes such as delamination, axial cracks, lamina bending and fibre fracturing were clearly evident.

- the pultruded composite tubes showed no sensitivity for strain rate, in the complete range of quasi-static to blast loading. This is due to the unidirectional fibre reinforcement.

Further, larger-scale blast tests have been conducted to understand the blast mitigation performance of a sacrifical cladding with an array of composite tubes. Tests have been conducted on two configurations of the composite tubes (25 and 37) with two charge masses of C4 (100 g and 150 g). From the conducted experimental tests the following conclusions can be made.

- The adopted concept of using two segments of concrete sewage pipes (4.2 m in length) provided a perfectly plane shock wave at the other end of the tube (crushing end). Furthermore, the negative phase of the blast load played a major role. It was observed

that the front skin panel was pulled back into the pipe during the negative phase. Hence, proper precautions should be taken to prevent the breakage of data measuring sensors and their wiring harness.

- The coupled numerical simulations using Autodyn predicted very close results compared to the experimental results. The peak reflected pressure, positive duration and the corresponding reflected impulse from the coupled numerical simulations were very close to the experimental results. The radial clearance between the front skin panel and the inner surface of the concrete pipe played a significant role for the total reflected impulse. Due to the clearing of the reflected pressure wave (through the radial clearance) the total reflected impulse was reduced. Hence, to predict accurate blast parameters the same experimental boundary conditions have to be used in the numerical model.

- The average peak crush load of the configuration 1 and 2 (25 and 37 composite tubes respectively) was 86.5 kN and 103.1 kN respectively. Progressive crushing was achieved for all tests and the transferred loads were reduced compared to the reference case.

- Local bending of the front skin panel and global bending of the rear skin panel were noticed. Due to that, the rear skin panel came into direct contact with the concrete wall for a longer time. As a result, a significant part of the load was directly transferred to the concrete wall. Therefore, there was a difference in the reflected impulse and the transferred impulse noticed. Hence, for future tests the rear skin panel (sandwich composite panel) should be replaced with an alternative material/structure with an adequate bending stiffness. However the weight of the skin panels should be very low to minimize the inertia effects.

Acknowledgements

References

[1]   S. Guruprasad and Abhijit Mukherjee, Layered sacrificial claddings under blast loading Part I -- analytical studies. International Journal of Impact Engineering, 2000. 24(9): p. 957-973.

[2]   S. Guruprasad and Abhijit Mukherjee, Layered sacrificial claddings under blast loading Part II -- experimental studies. International Journal of Impact Engineering, 2000. 24(9): p. 975-984.

[3]   C.Derdas and V.Kostopoulos C.Kotzialis, Blast behaviour of plates with sacrificial cladding. 5th GRACM International congress on computational mechanics, 2005.

[4]   A. G. Hanssen, L. Enstock and M. Langseth, Close-range blast loading of aluminium foam panels. International Journal of Impact Engineering, 2002. 27(6): p. 593-618.

[5]   C. Kotzialis, C. Derdas and V. Kostopoulos, Blast behaviour of plates with sacrificial cladding. 5th GRACM International congress on computational mechanics, June 29 - July 1, Limassol, Cyprus., 2005.

[6]   M. D. Theobald and G. N. Nurick, Experimental and numerical analysis of tube-core claddings under blast loads. International Journal of Impact Engineering. 37(3): p. 333-348.

[7]   Starr, C.M. and Krauthammer, T. (2005). Cladding-structure interaction under impact loads. Journal of Structural Engineering – ASCE, 131(8), 1178-1185.

[8]   A. G. Mamalis, D. E. Manolakos and G. A. Demosthenous, *Crushing behaviour of thin-walled, non-circular, glass fibre-reinforced composite tubular components due to bending.* Composites, 1992. **23**(6): p. 425-433.

[9]   A. G. Mamalis, D. E. Manolakos, G. A. Demosthenous and M. B. Ioannidis, *Energy absorption capability of fibreglass composite square frusta subjected to static and dynamic axial collapse.* Thin-Walled Structures, 1996. **25**(4): p. 269-295.

[10]   A. G. Mamalis, D. E. Manolakos, M. B. Ioannidis and D. P. Papapostolou, *Crashworthy characteristics of axially statically compressed thin-walled square CFRP composite tubes: experimental.* Composite Structures, 2004. **63**(3-4): p. 347-360.

[11]   A. G. Mamalis, M. Robinson, D. E. Manolakos, G. A. Demosthenous, M. B. Ioannidis and J. Carruthers, *Crashworthy capability of composite material structures.* Composite Structures, 1997. **37**(2): p. 109-134.

[12]   S. Solaimurugan and R. Velmurugan, *Progressive crushing of stitched glass/polyester composite cylindrical shells.* Composites Science and Technology, 2007. **67**(3-4): p. 422-437.

[13]   G L and Jones Farley, R.M, *Analogy for the effect of material and geometrical variables on energy absorption capability of composite tubes.* Journal of Composite Materials, 1992. **26**: p. 78.

[14]   P. H. Thornton, *The crush behavior of pultruded tubes at high strain rates.* Journal of Composite Materials, 1989. **24**: p. 22.

[15]   H. Hamada, J. C. Coppola, D. Hull, Z. Maekawa and H. Sato, *Comparison of energy absorption of carbon/epoxy and carbon/PEEK composite tubes.* Composites, 1992. **23**(4): p. 245-252.

[16]   S. Ramakrishna and D. Hull, *Energy absorption capability of epoxy composite tubes with knitted carbon fibre fabric reinforcement.* Composites Science and Technology, 1993. **49**(4): p. 349-356.

[17]   S. Chung Kim Yuen and G. N. Nurick, The energy absorbing characteristics of tubular structures with geometric and material modifications: an overview, Applied Mechanics Reviews, Volume 61 (2008). 020802 (15 pages)

[18]   D. Karagiozova, G. N. Nurick, S. Chung Kim Yuen, Energy absorption of aluminium alloy circular and square tubes under an axial explosive load, Thin-Walled Structures, Volume 43 (2005), 956-982.

[19]   M. D. Theobald and G. N. Nurick Numerical investigation of the response of sandwich-type panels using thin-walled tubes subject to blast loads, International Journal of Impact Engineering, Volume 34 (2007), 134-156.

[20]   C. J. McGregor, R. Vaziri, A. Poursartip, X. Xiao, Simulation of progressive damage development in

braided composite tubes under axial compression, Composites Part A: Applied Science and Manufacturing, Volume 38 (2007), 22472259.

[21]   Palanivelu, S., Van Paepegem, W., Degrieck, J., Van Ackeren, J., Kakogiannis, D., Van Hemelrijck, D., Wastiels, J. and Vantomme, J. (2010). Experimental study on the axial crushing behaviour of pultruded composite tubes. Polymer Testing, 29(2), 224-234.

[22]   Palanivelu, S., Van Paepegem, W., Degrieck, J., Kakogiannis, D., Van Ackeren, J., Van Hemelrijck, D., Wastiels, J. and Vantomme, J. (2010). Comparative study of the quasi-static energy absorption of small-scale composite tubes with different geometrical shapes for use in sacrificial cladding structures. Polymer Testing, 29(3), 381-396.

[23]   Palanivelu, S., Van Paepegem, W., Degrieck, J., Vantomme, J., Kakogiannis, D., Van Ackeren, J., Van Hemelrijck, D. and Wastiels, J. (2010). Comparison of the crushing performance of hollow and foam-filled small-scale composite tubes with different geometrical shapes for use in sacrificial cladding structures. Composites Part B: Engineering, 41(6), 434-445.

[24]   Palanivelu, S., Van Paepegem, W., Degrieck, J., Vantomme, J., Kakogiannis, D., Van Ackeren, J., Van Hemelrijck, D. and Wastiels, J. (2011). Crushing and energy absorption performance of different geometrical shapes of small-scale glass/polyester composite tubes under quasi-static loading conditions. Composite Structures, 93(2), 992-1007.

[25]   Palanivelu, S., Van Paepegem, W., Degrieck, J., Kakogiannis, D., Van Ackeren, J., Van Hemelrijck, D., Wastiels, J. and Vantomme, J. (2010). Parametric study of crushing parameters and failure patterns of pultruded composite tubes using cohesive elements and seam. Part I –Central delamination and triggering modelling. Polymer Testing, 29(6), 729-741.

[26]   Palanivelu, S., Van Paepegem, W., Degrieck, J., Van Ackeren, J., Kakogiannis, D., Wastiels, J., Van Hemelrijck, D., and Vantomme, J. (2010). Parametric study of crushing parameters and failure patterns of pultruded composite tubes using cohesive elements and seam. Part II – Multiple delaminations and initial geometric imperfections. Polymer Testing, 29(7), 803-814.

[27]   Kakogiannis, D., Chung Kim Yuen, S., Palanivelu, S., Van Hemelrijck, D., Van Paepegem, W., Wastiels, J., Vantomme, J. and Nurick, G.N. (2013). Response of pultruded composite tubes subjected to dynamic and impulsive axial loading. Composites Part B: Engineering, 55, 537-547.

[28]   Thornton, P. H., The crush behavior of pultruded tubes at high strain rates. Journal of Composite Materials, 1989. 24: p. 22.

Table 1: Comparison of experimental measurements and calculated blast parameters from Autodyn simulations without and with a radial clearance between the front skin panel and the concrete pipe for a charge mass of 150 g C4.

Parameters	Pressure sensor 1	Pressure sensor 2	Pressure sensor 3
Experimental			
Peak reflected pressure (kPa)	561.5	525.2	530.8
Positive duration (ms)	5.2	4.9	5.1
Reflected impulse (kPa.ms)	627.1	685.3	737.6
Numerical simulation without considering the radial clearance			
Peak reflected pressure (kPa)	590		
Positive duration (ms)	6.2		
Reflected impulse (kPa.ms)	908		
Numerical simulation with considering the radial clearance			
Peak reflected pressure (kPa)	564		
Positive duration (ms)	5.24		
Reflected impulse (kPa.ms)	679		

Table 2: Dimensional and material details of the composite tube series.

Cross-section	Fibre	Resin	Dimensions (mm)	ρ_{linear} (g/mm)	Volume fraction (%)
Circular	Glass	Polyester	$\phi = 22$ $t = 1$ $L = 100$	0.14 without foam 0.15 with foam	$V_m = \sim 50$ $V_f = \sim 50$
ϕ - Outer diameter; t – thickness; L – length of tube; V_m – volume fraction of matrix; V_f – volume fraction of fibre.					

Table 3: Summary of crushing parameters.

Charge mass	No. composite tubes	Stand-off distance	Load cells data	Peak crush load	Total peak crush load	Time for load transfer	Average time	Reflected impulse (from Autodyn)	Transferred impulse	Total transferred impulse	Average deformation length
(g)		(m)		(kN)	(kN)	(ms)	(ms)	(kN.ms)	(kN.ms)	(kN.ms)	(mm)
Test with configuration 1 (25 composite tubes)											
100	25	4.2	Load cell 1	29.5					85.2		
			Load cell 2	32.3	87.7		8.2	599	88.1	249.3	25.8
			Load cell 3	25.9					76.0		
150	25	4.2	Load cell 1	25.4		8.1			87.3		
			Load cell 2	30.1	86.6	8.0	8.4		89.9	267.3	33.6
			Load cell 3	31.1		9.2		679	90.1		
			Load cell 1	36.1		11.6			95.0		
			Load cell 2	27.2	85.4	10.0	10.7		71.1	247.3	31.1
			Load cell 3	22.1		10.7			81.2		
Test with configuration 2 (37 composite tubes)											
150	37	4.2	Load cell 1	30.3		10.4			72.5		
			Load cell 2	38.1	104.4	7.15	9.4		53.8	196.1	55.2
			Load cell 3	36.0		10.8		679	69.8		
			Load cell 1	27.5		8.16			65.9		
			Load cell 2	40.9	101.9	10.7	8.95		61.0	185.2	49.8
			Load cell 3	33.5		7.99			58.3		
Reference test											
150	-	4.2	Load cell 1	48.5		5.4			87.9		
			Load cell 2	46.9	138.3	3.6	4.4	679	83.4	256.6	-
			Load cell 3	42.9		4.2			85.3		

Figure Captions

Figure 1: Working principle of a sacrificial cladding structure.

Figure 2: (a) Schematic view (b) Small-scale air blast test set-up.

Figure 3: Uniform progressive crushing of the circular cross sectional glass polyester composite tubes (1 mm wall thickness) : tube 1 and 2 (30 g and 30 cm stand-off distance) and tube 3, 4 and 5 (20g and 30 cm stand-off distance).

Figure 4: Progressive deformation patterns of commercially available pultruded GFRP composite tubes (2 mm wall thickness) for free air blast loading (40g of C4) with 15 cm stand-off distance.

Figure 5: (a) Pendulum set-up for contact blast loading, (b) progressive deformation patterns of GFRP composite tubes subjected to contact blast loading condition.

Figure 6: Comparison of force-deformation curves for different loading conditions (quasi-static, impact and blast loading).

Figure 7: 2D wedge model with incident overpressure contours for 20g of C4 at 30 cm stand-off distance.

Figure 8: Comparison of incident pressure-time histories from Autodyn, ConWep and experimental measurements for 20g of C4 at 30 cm stand-off distance.

Figure 9: Coupled 3D simulation of the blast detonation and interaction with the test set-up.

Figure 10: Interaction of blast pressure waves with the aluminium skin plate.

Figure 11: Interaction of the reflected pressure wave with the skin plate from the ground surface.

Figure 12: Experimental proof of the "clearing" of the shock wave around the edges of the skin plate for 20 g TNT at 30 cm stand-off distance.

Figure 13: Schematic representation of the experimental set-up for the sacrifical cladding.

Figure 14: Large-scale blast experimental test set-up: (a) sandwich skin panel with composite tubes (25 tubes configuration) (b) Side view of assembly

Figure 15: Schematic drawing of the sandwich skin plates with glass/polyester face sheets and Divinycell P foam.

Figure 16: Autodyn simulation of the propagation of the blast pressure wave inside the concrete sewage pipes for 150 g C4.

Figure 17: Comparison of the experimentally measured and numerically calculated (reflected) pressure time histories for 150 g C4 considering a radial clearance between the front skin panel and concrete pipe.

Figure 18: (a) Quasi-static progressive crushing modes of composite tubes with uniform thickness of 1 mm and the corresponding load-deformation curves, (b) Load-deformation curves for two identical tubes under quasi-static loading.

Figure 19: Global deformation patterns of the composite tubes (a) configuration 1 (25 composite tubes) with 150 g of C4 (b) configuration 2 (37 composite tubes) with 150 g of C4.

Figure 20: Final deformation patterns of composite tubes (a-b) for 150 g of C4 with configuration 1 (25 composite tubes). (c-d) for 150 g of C4 with configuration 2 (37 composite tubes)

Figure 21: Transferred load time histories (a) for 100 g of C4 with 25 tubes (b) for 150 g of C4 with 25 tubes (c) for 150 g of C4 with 37 tubes.

Figure 22: Image sequence of crushing of 25 composite tubes (150 g C4).

Figure 23: Compressive crushing characteristic of the divinycell P foam.

Figure 24: Tensile and compressive failures of back face of rear skin panel (a) fibre tensile failure (b) fibre compressive failure (c) matrix tensile failure (d) matrix compressive failure (magnification factor 5).

Figure 25: Fibre and matrix failures of bottom face of the top skin panel (a) fibre tensile failure (b) matrix tensile failure (magnification factor 5).

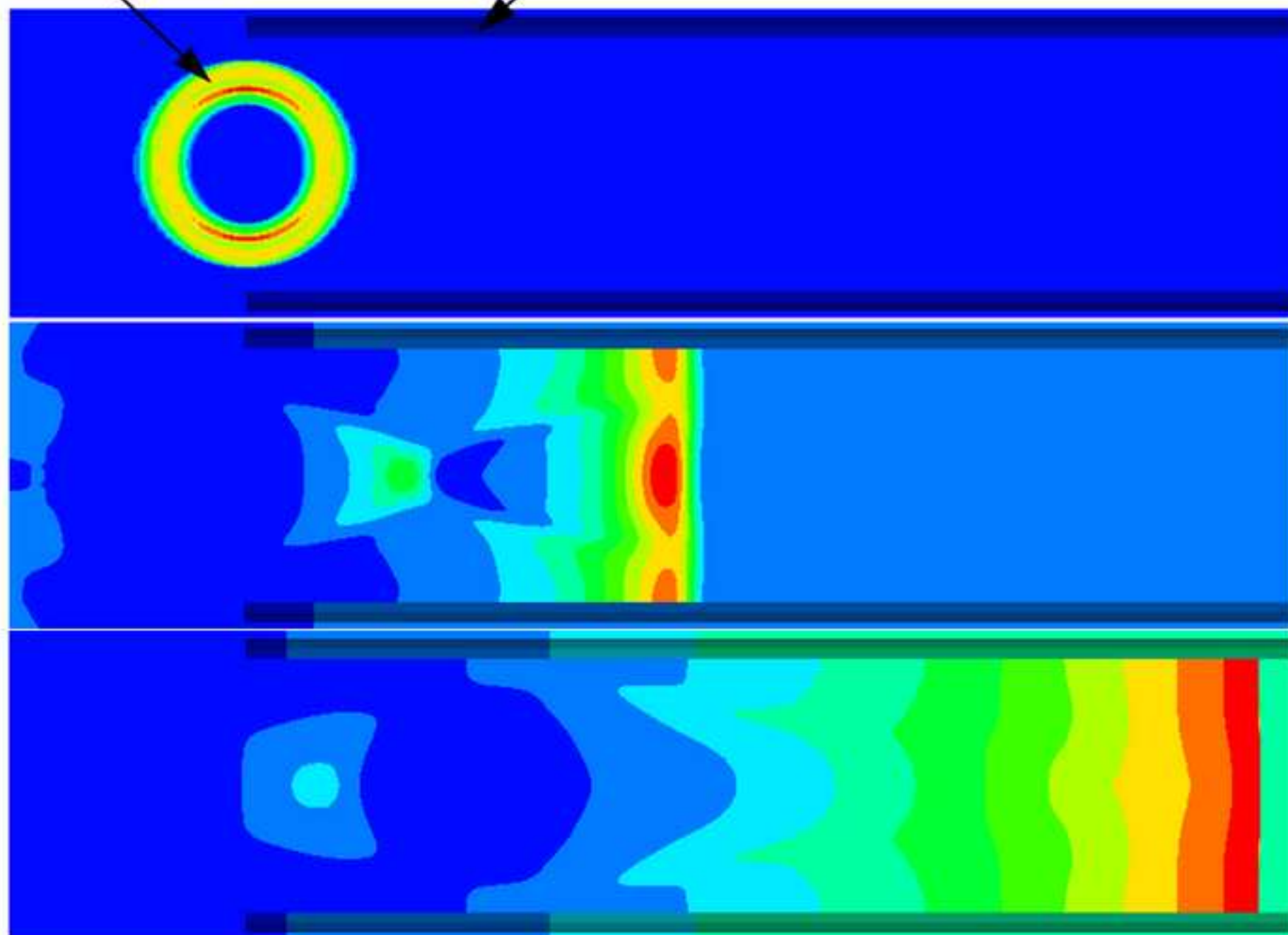Figure 26: Stress distribution on core foam (divinycell P foam) of the rear skin panel (magnification factor 5).

Figure 01
Click here to download high resolution image

Charge (C4)

Z

Z

Blast pressure

Pressure sensor (to measure
the incident pressure)

Accelerometer

Bottom resting plate

Vent for air out

Fixture

Aluminium skin plate

Pressure sensor (to measure
the reflected pressure)

Composite tube

Dynamic load cell

Side cover tube

Bottom copper tube

(a)

(b)
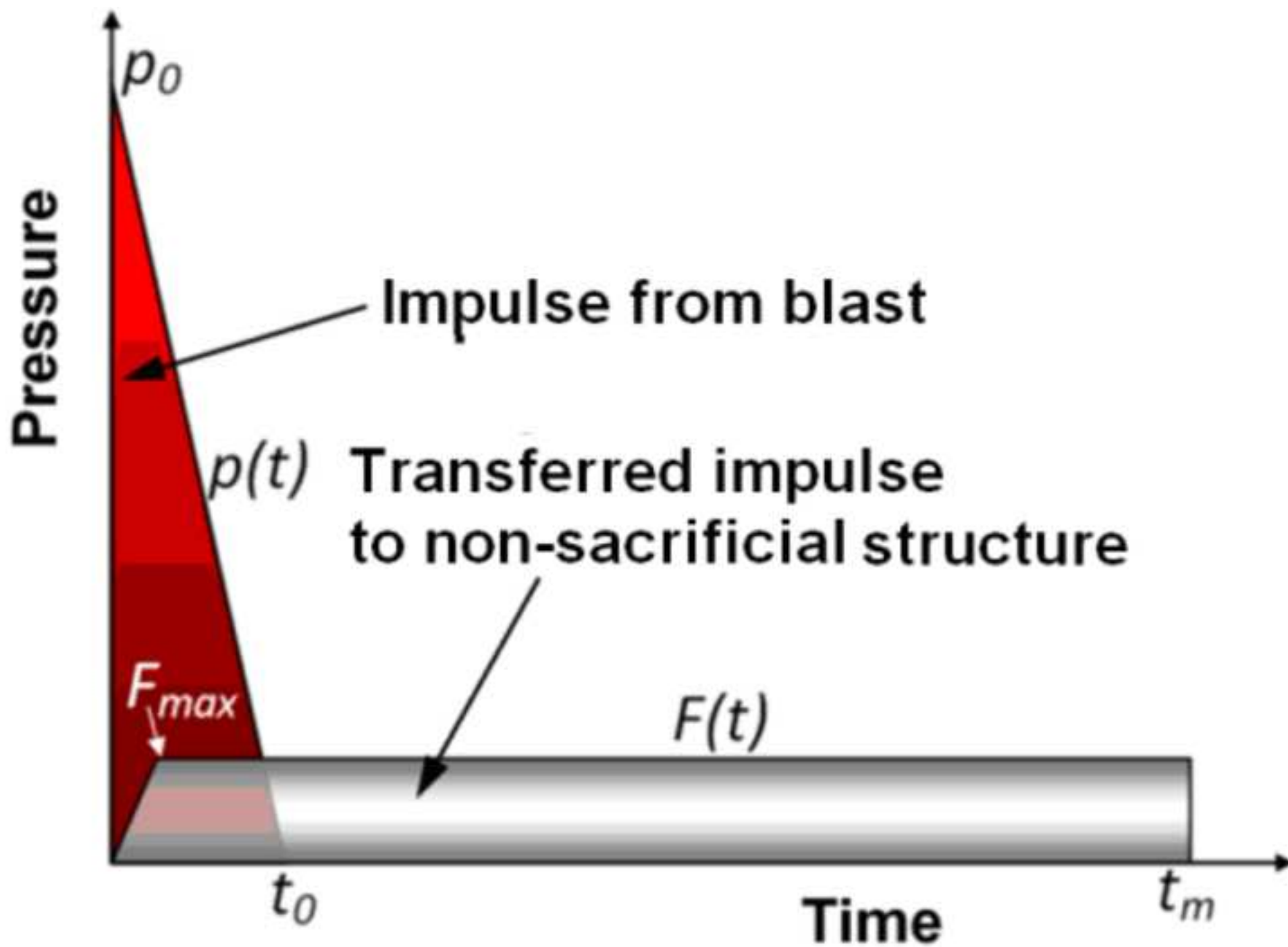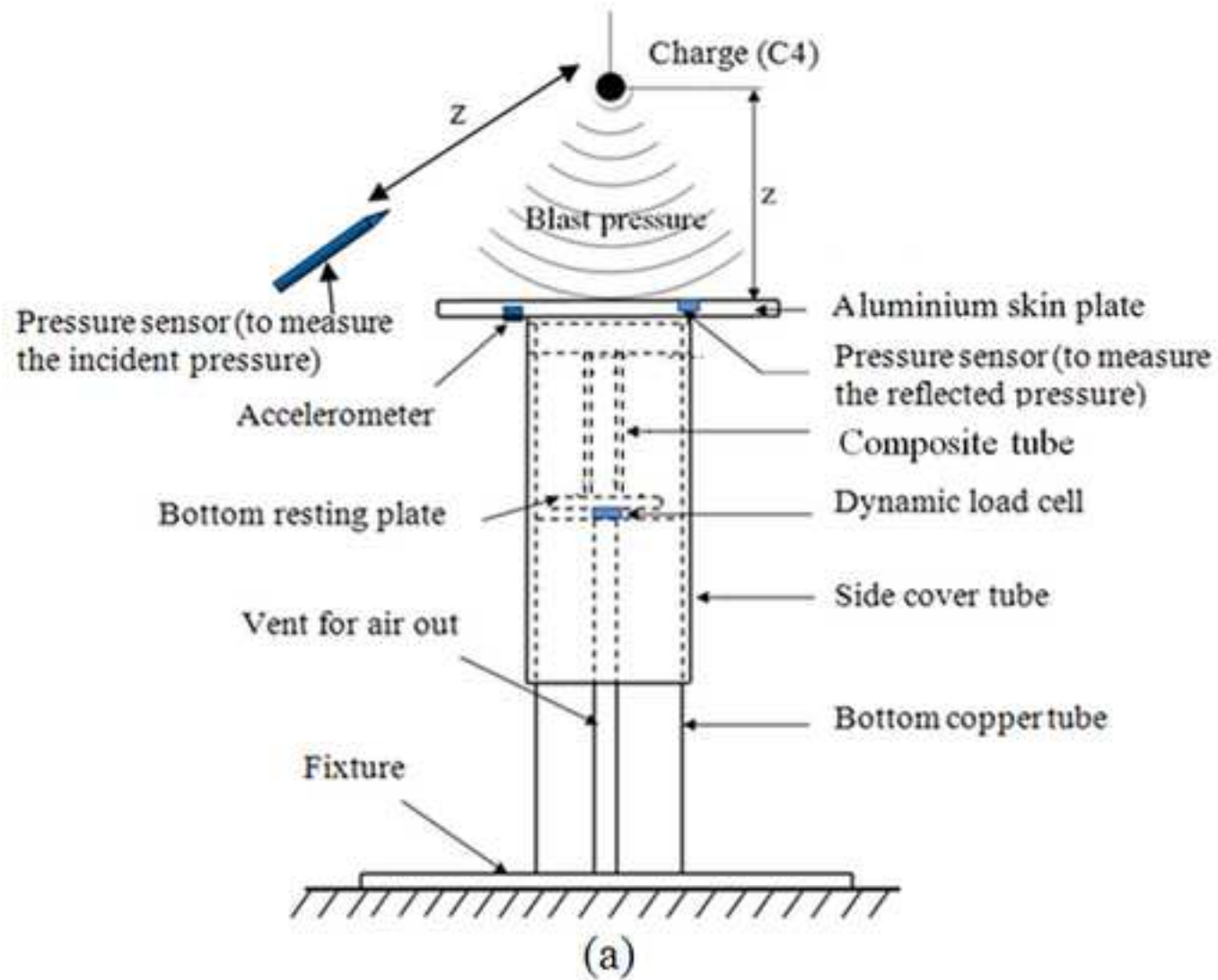
Figure 03
Click here to download high resolution image
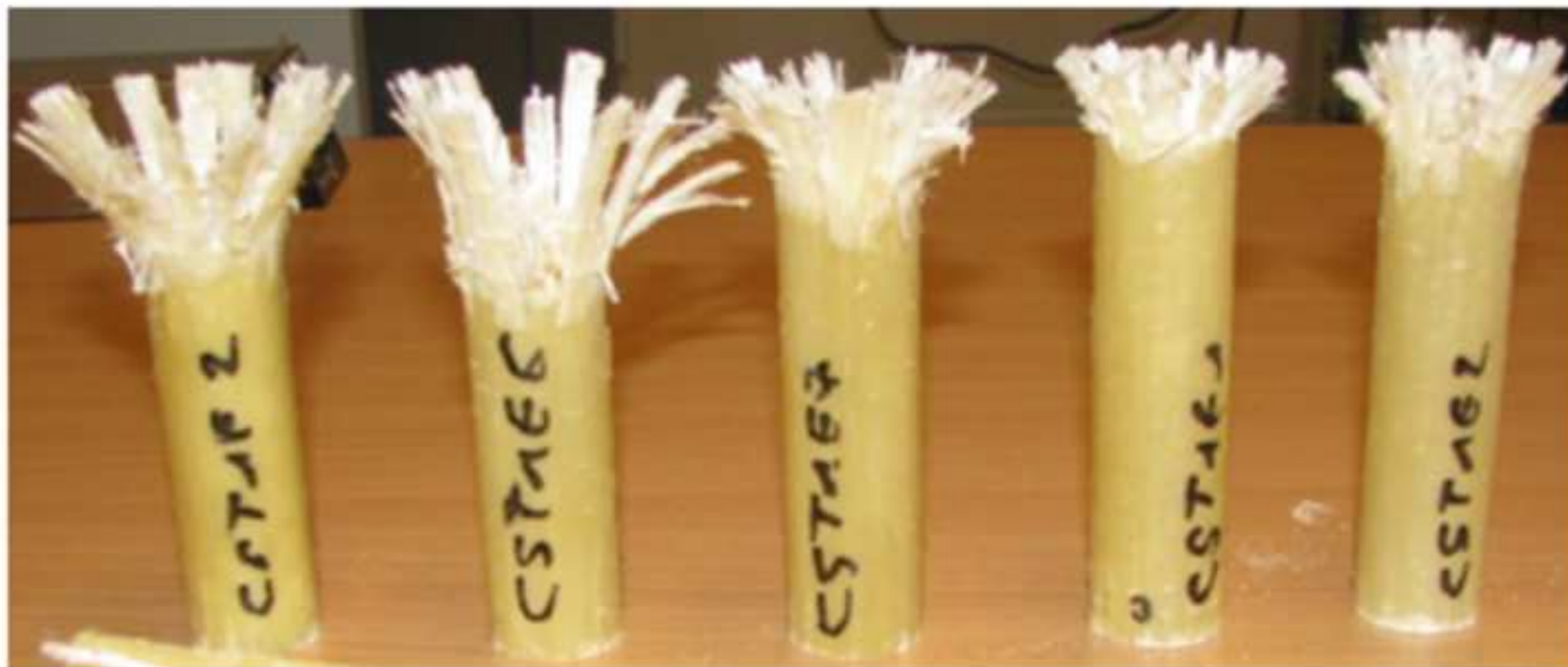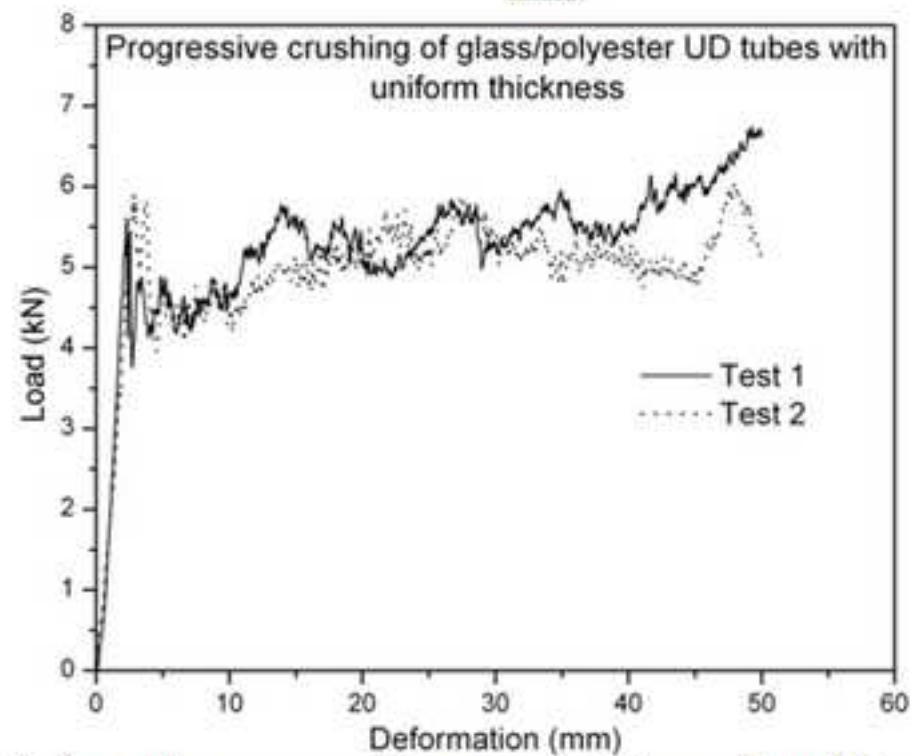
Figure 04
[Click here to download high resolution image](#)
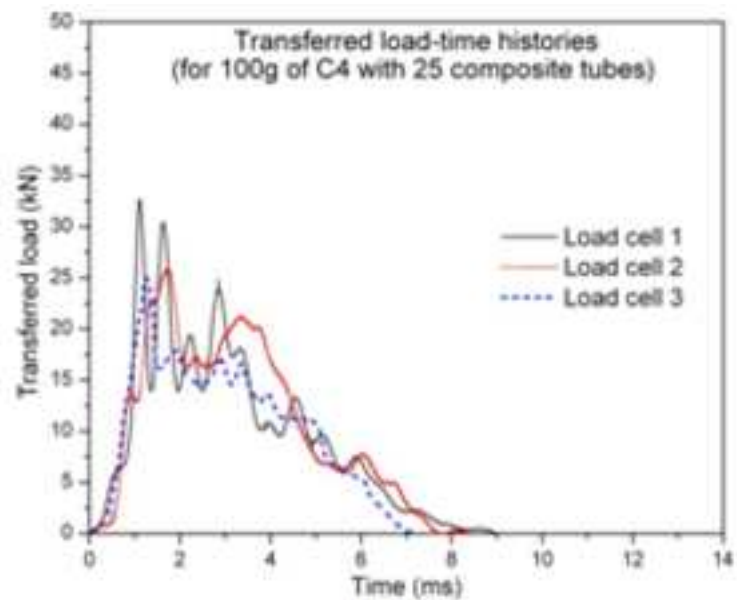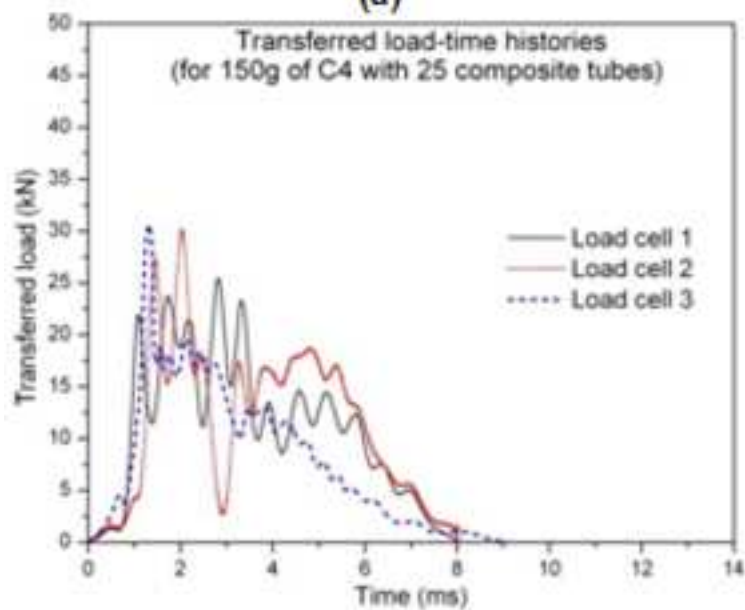
Figure 05
Click here to download high resolution image

(a)   (b)

Figure 06
Click here to download high resolution image
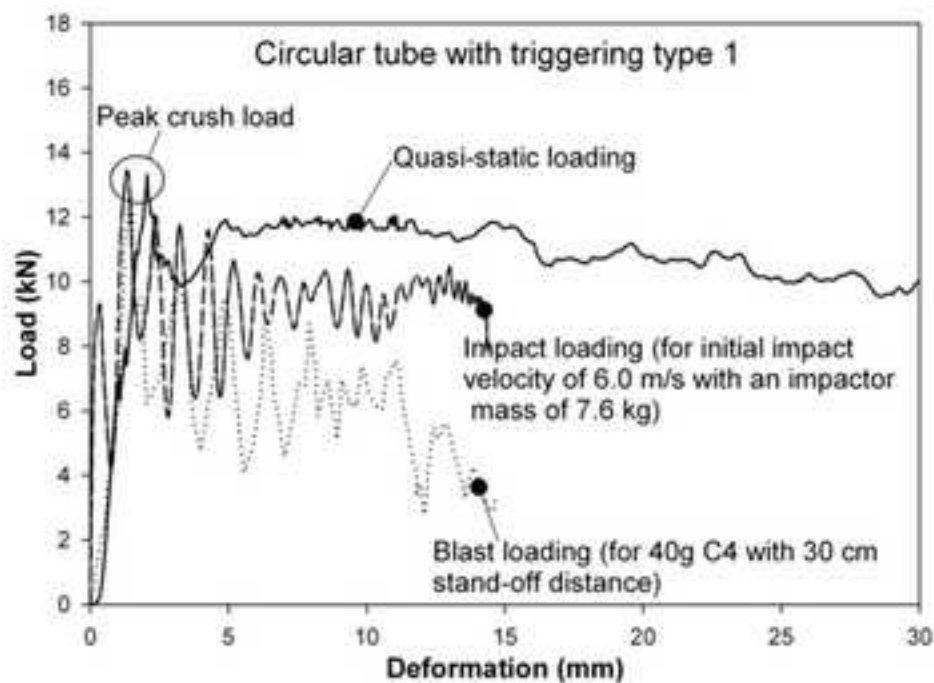
(a) Triggering type 1
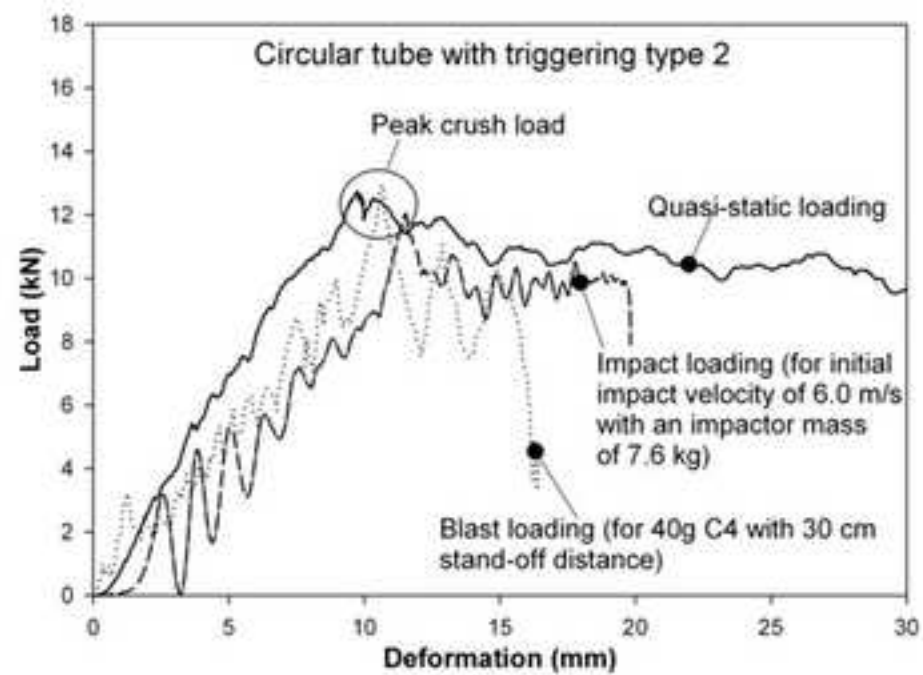
(b) Triggering type 2

Figure 07
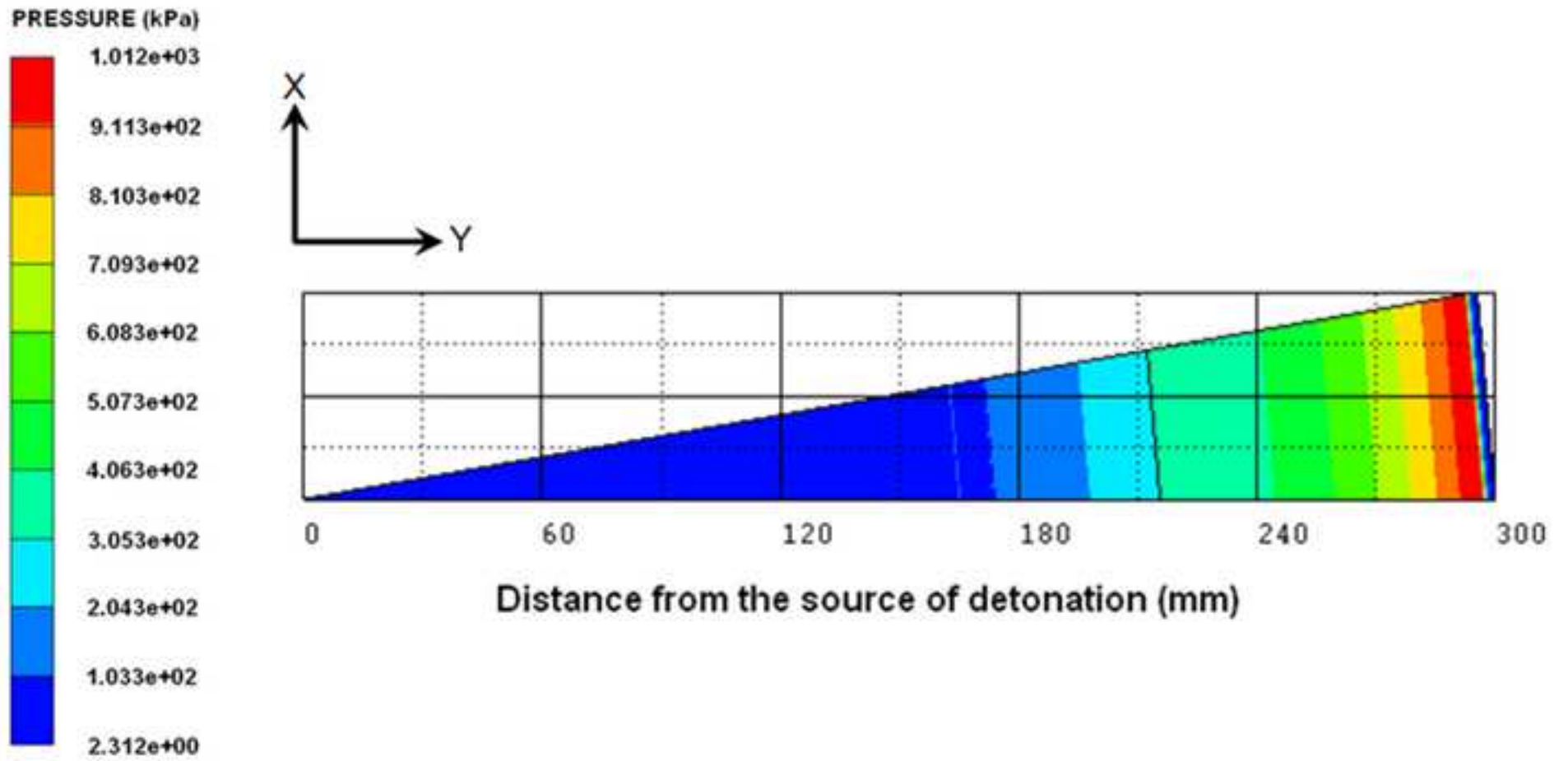
Figure 08
Click here to download high resolution image

Comparison of incident pressure

Experimentally measured (test 1 with aluminium skin plate (ϕ 250 mm; 1.187kg; R_a = 7 μm)

.... Calculated from Autodyn

- - - Predicted from ConWep

Peak pressure

Positive phase duration from experiment and Autodyn

Positive phase duration from ConWep

Atmospheric pressure line
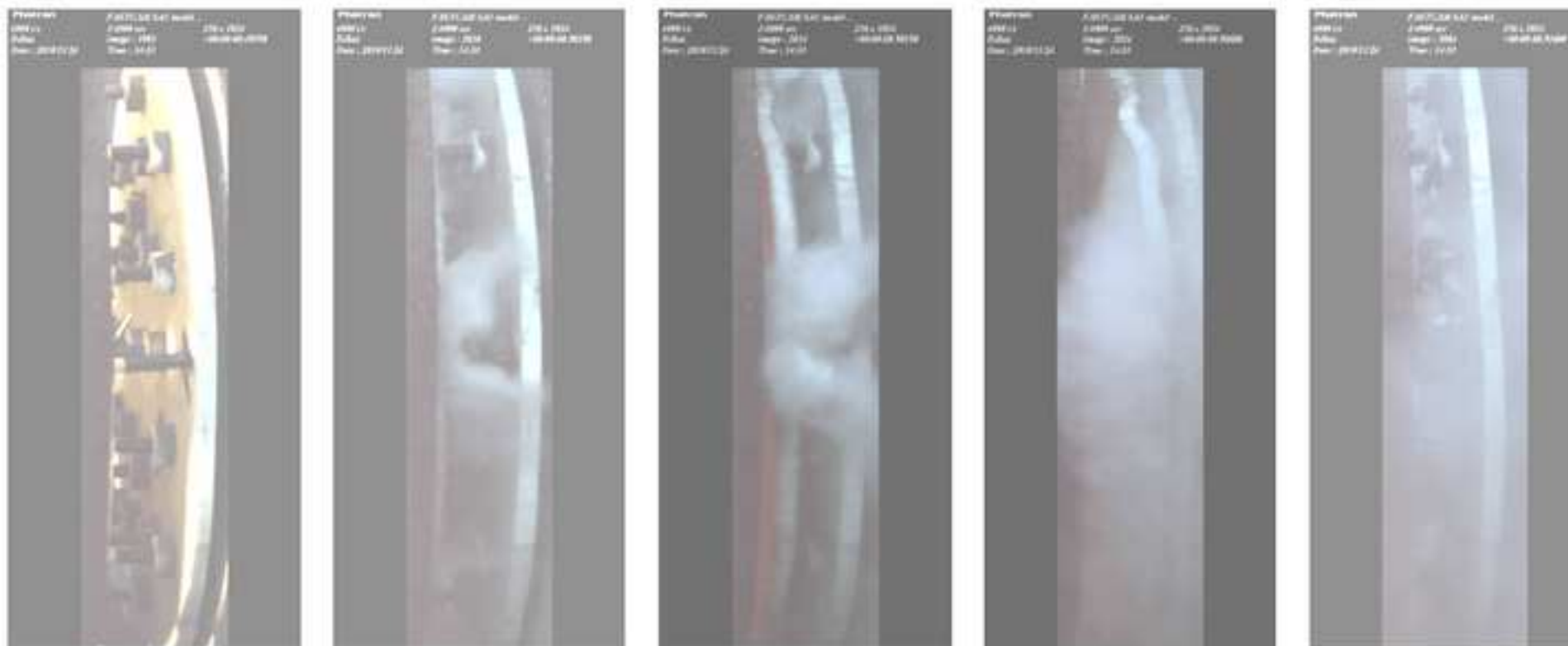
Incident pressure (kPa)

Time (ms)
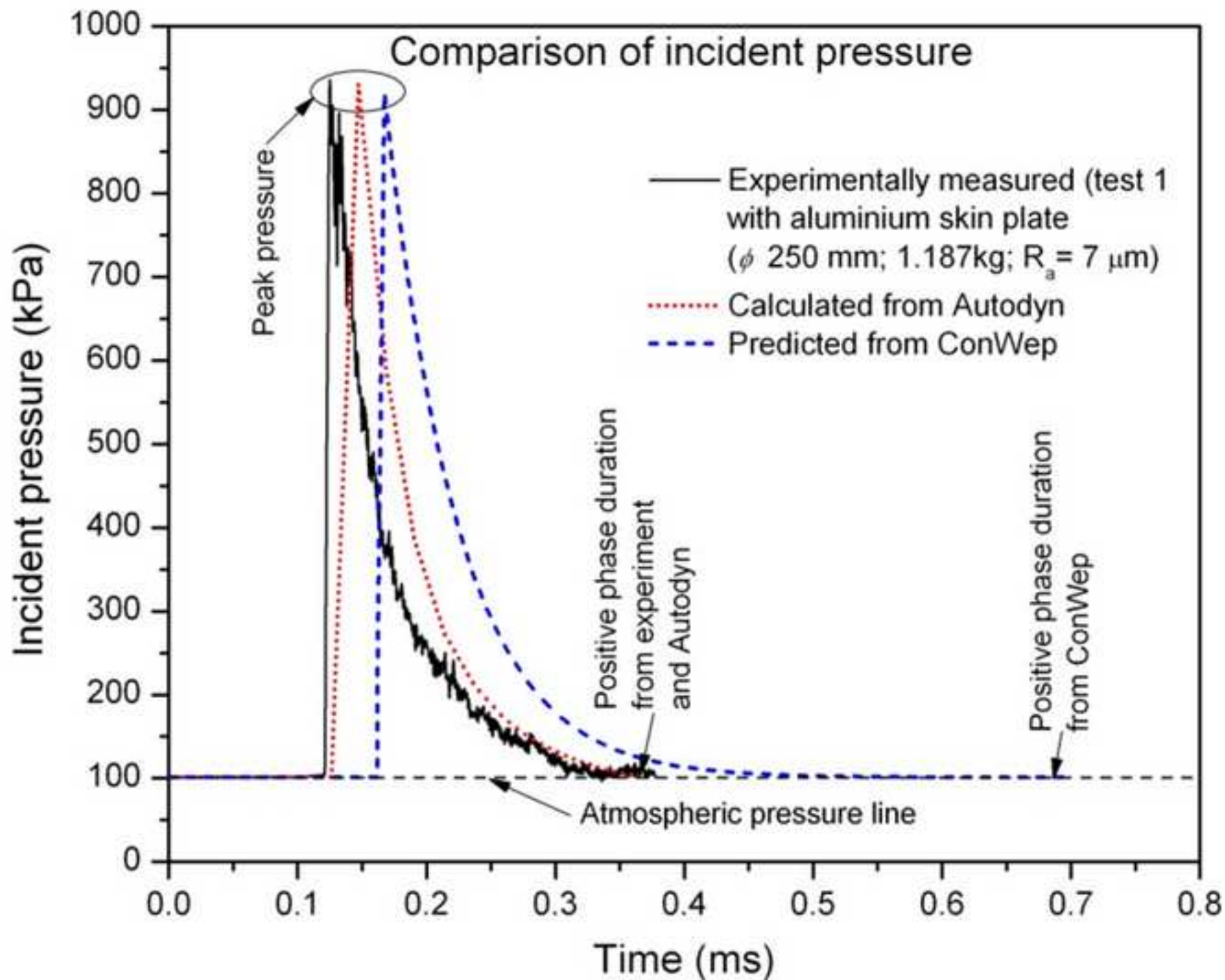
Figure 09
Click here to download high resolution image
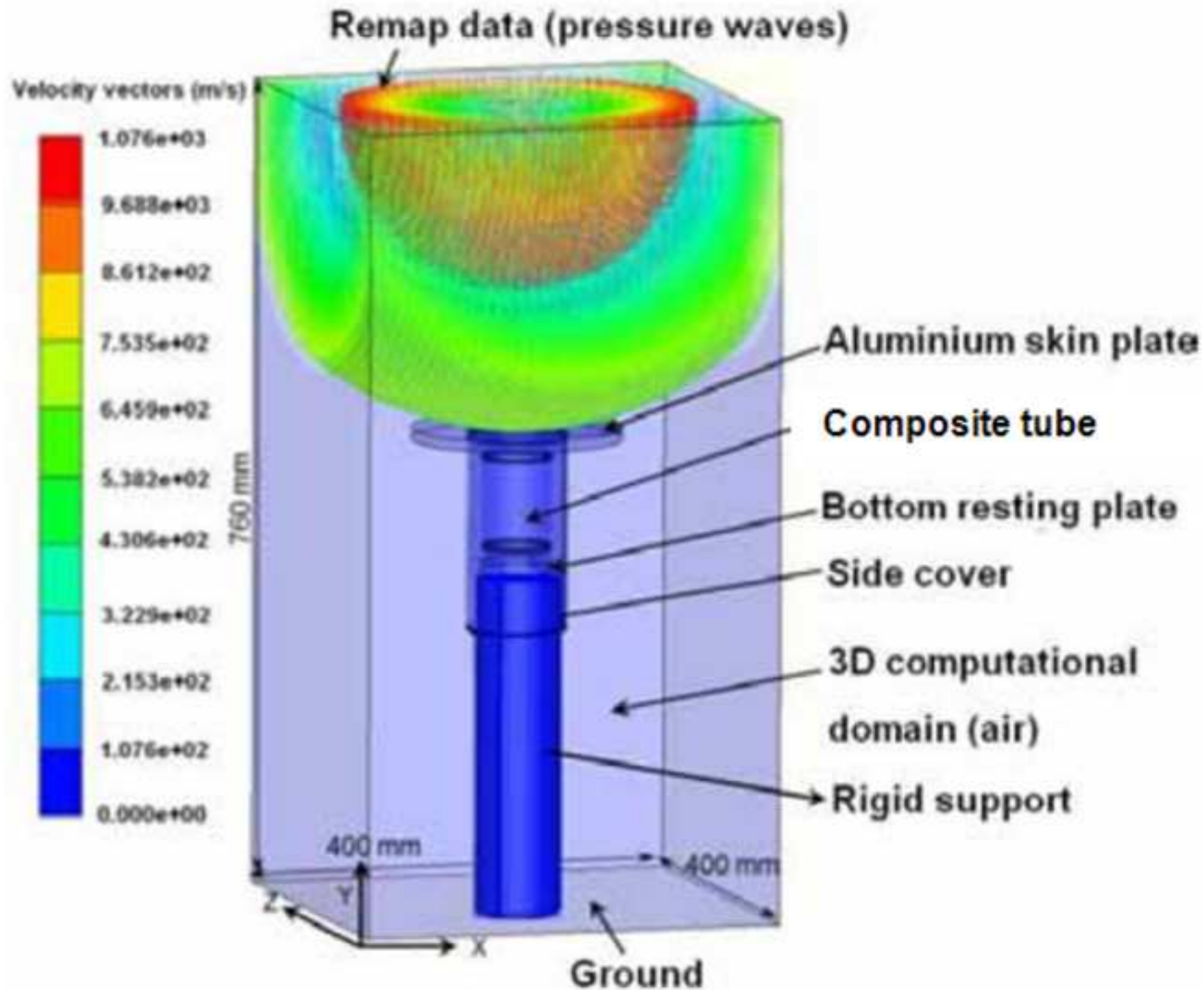
Figure 09

Figure 10
Click here to download high resolution image
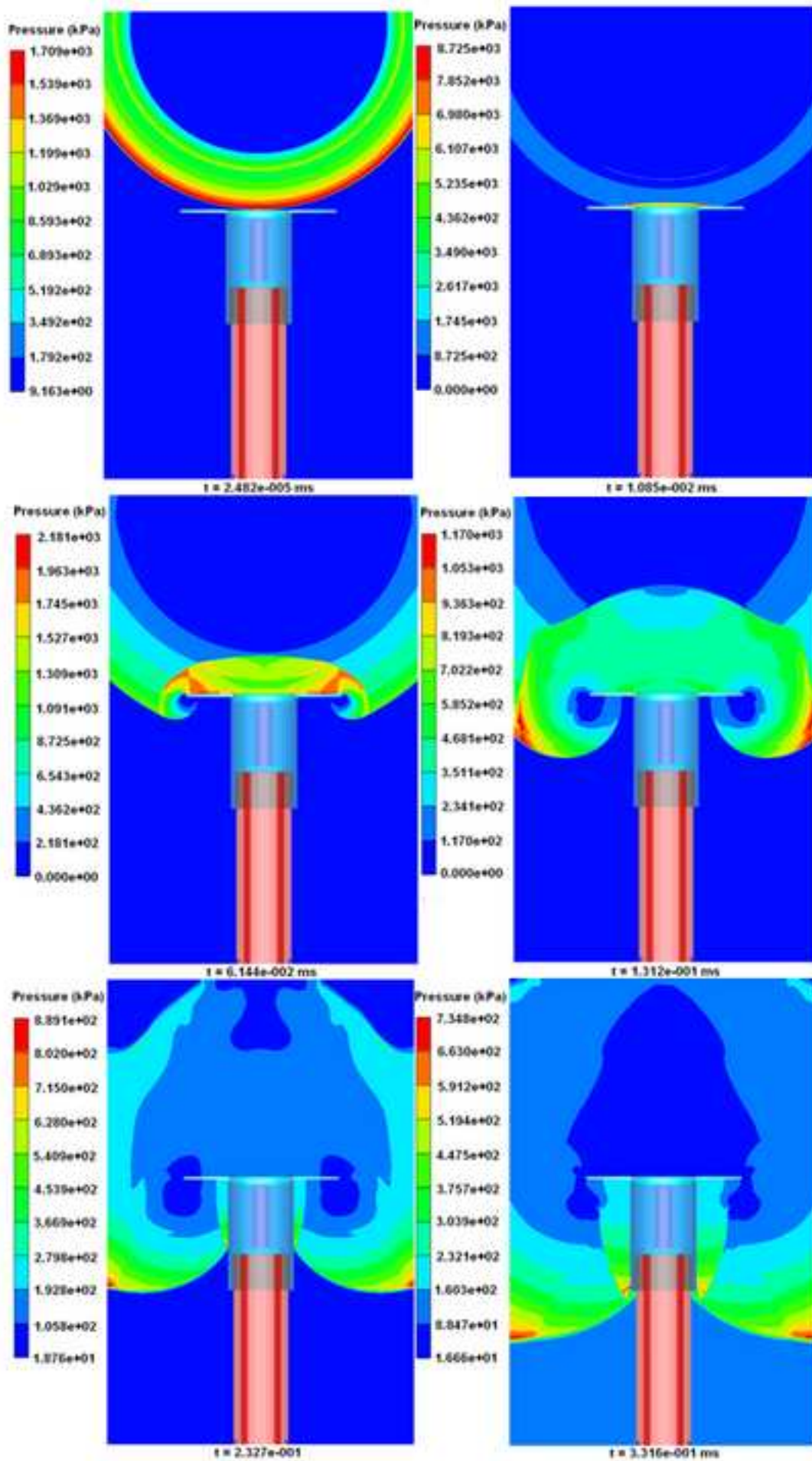
Figure 11
Click here to download high resolution image
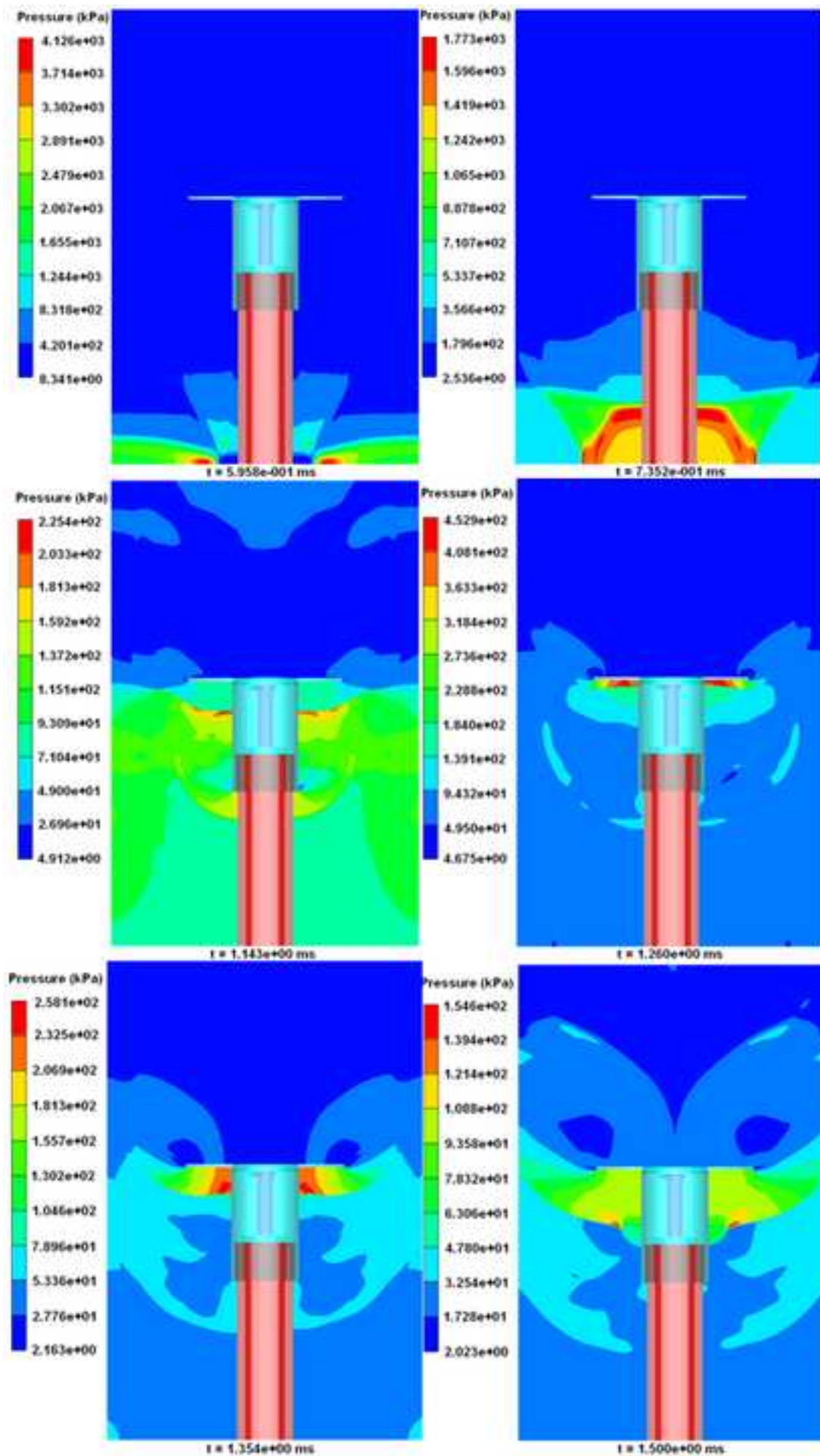
Figure 12

Figure 13
Click here to download high resolution image

Test specimens   Accelerometers in the front skin plate

Dynamic force sensors behind the back plate

4.2 m

Charge (C4)

Global view of the experimental test set-up

Pressure sensors (to measure the reflected pressure) in the front skin plate
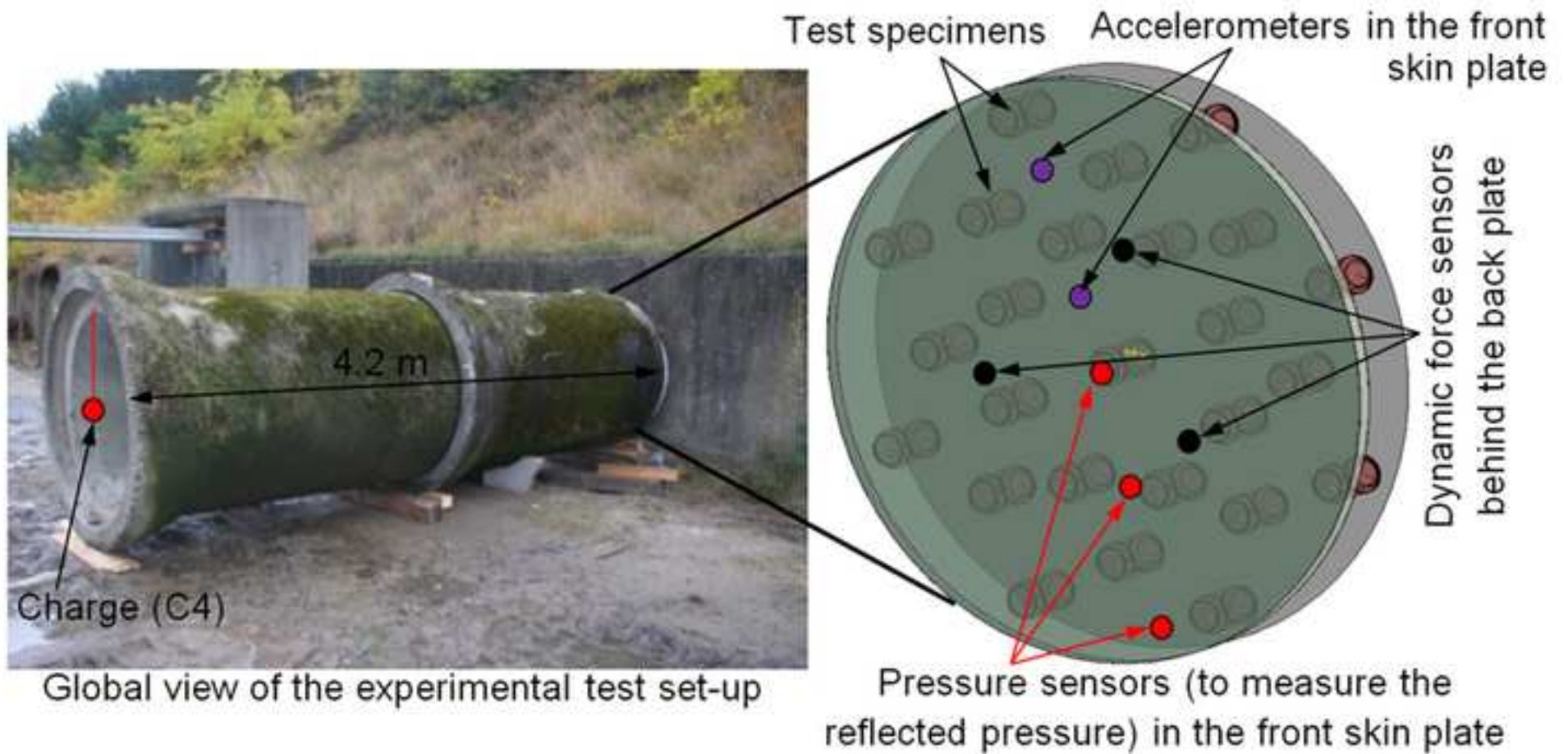
Figure 14
Click here to download high resolution image

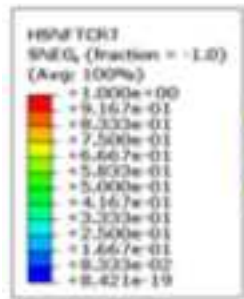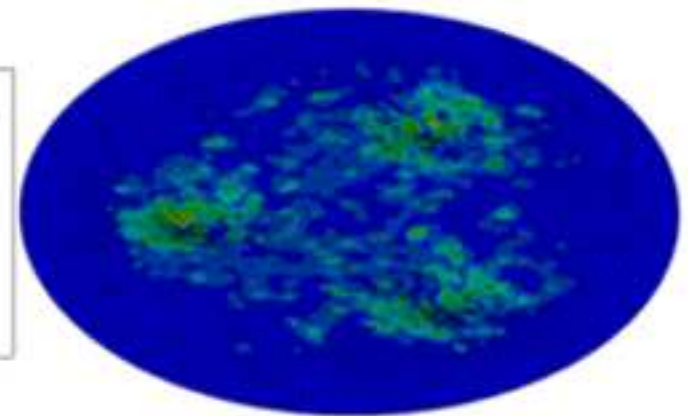(a)   (b)
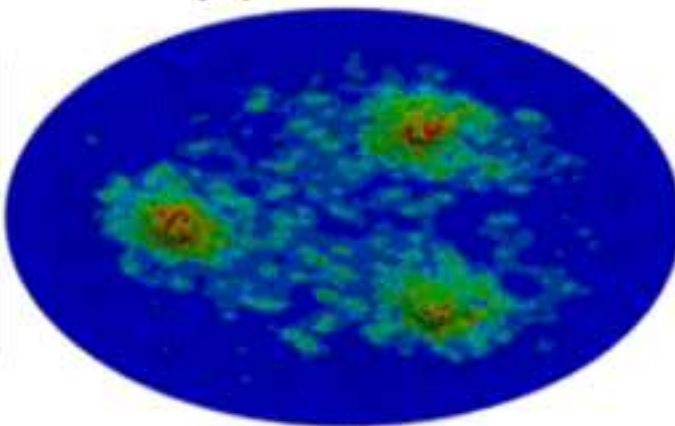
Divinycell P foam

Glass fibre

Aramid stitch

Figure 16
Click here to download high resolution image

Comparison of the reflected pressure-time histories
(for 150g of C4) considering radial clearance

Numerical peak pressure
(average ~ 564 kPa)

Experimental peak pressures
(average ~ 550 kPa)

—— Experimental pressure gauge 1
—— Experimental pressure gauge 2
—— Experimental pressure gauge 3
—— Numerical simulation (Autodyn)
   (average pressure curve) considering
   radial clearance
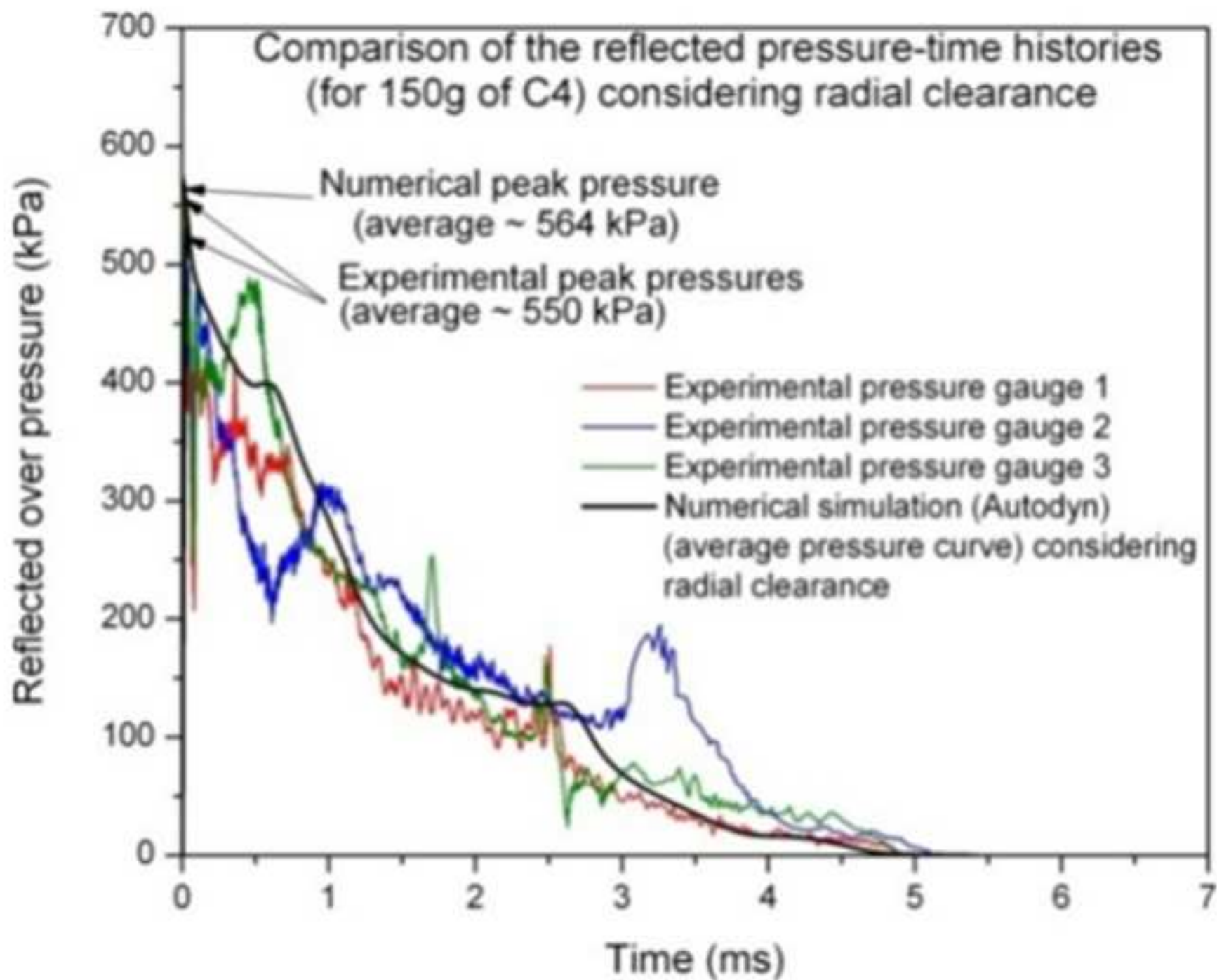
Figure 18
Click here to download high resolution image
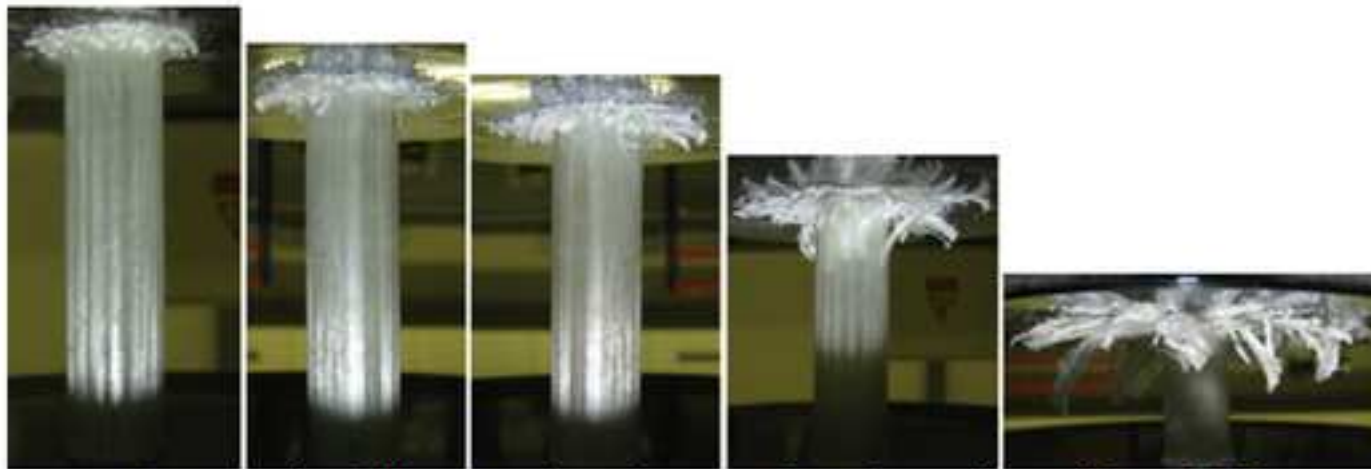
(a) Progressive failure modes of composite tubes with uniform thickness of 1 mm.

(b) Load-deformation curves of composite tubes with uniform thickness of 1 mm.

(a)   (b)
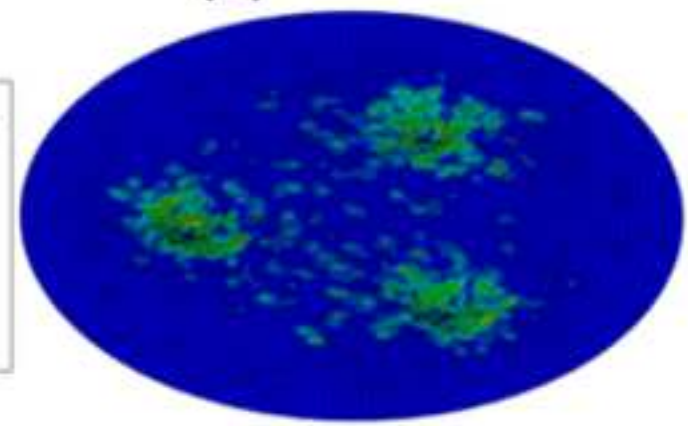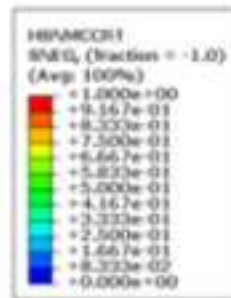
Figure 20
Click here to download high resolution image

(a)

(b)

(c)

(d)

(a)

(b)

(c)
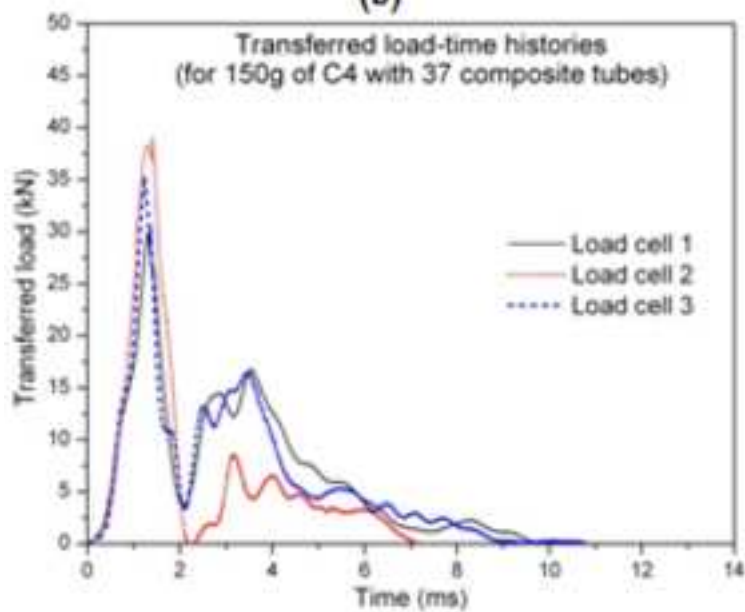
Figure 22

Figure 23
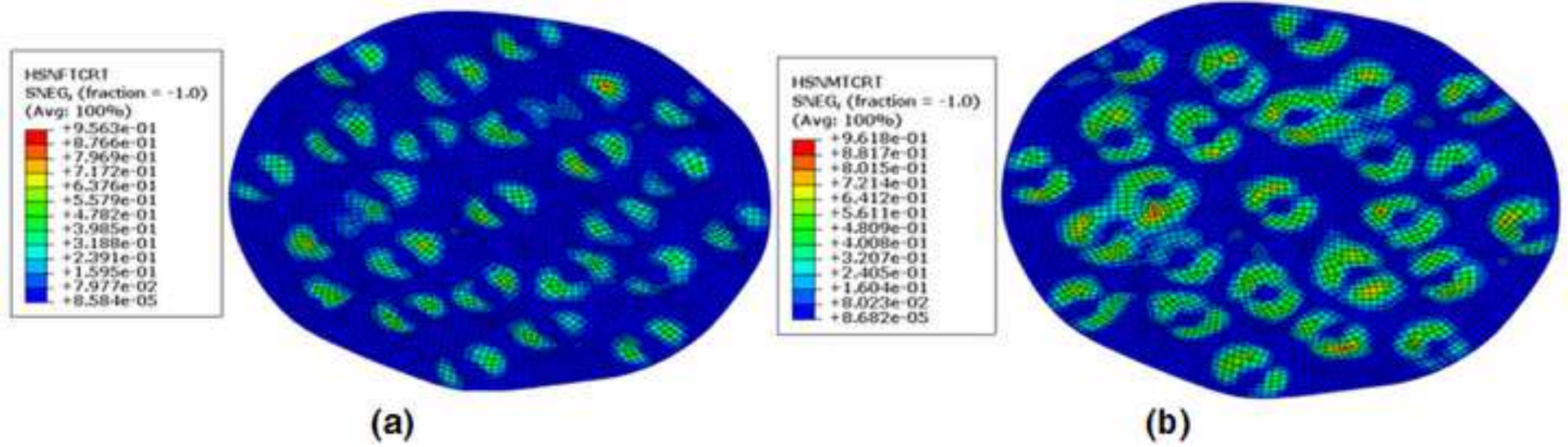**Click here to download high resolution image**
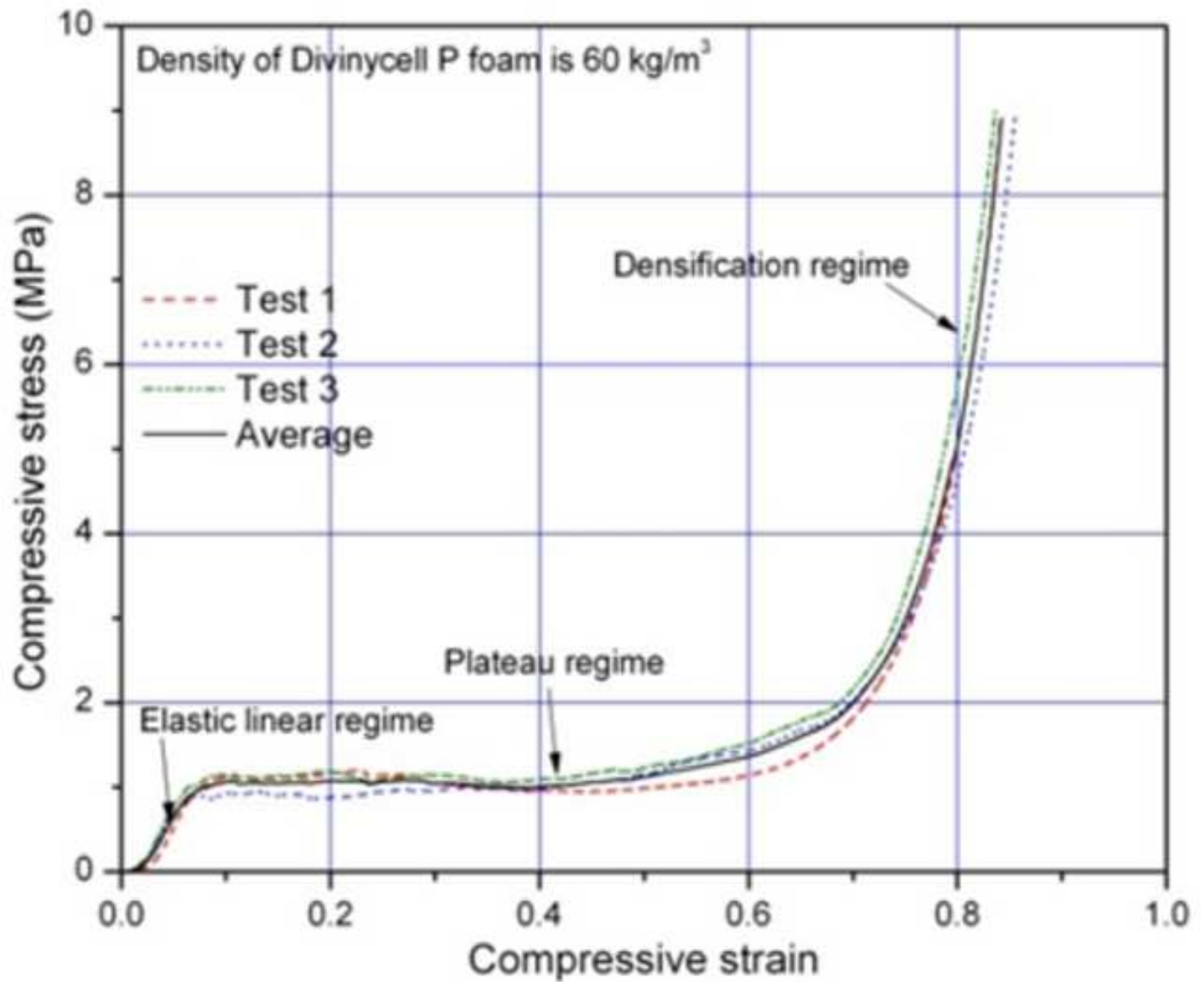
(a)

(b)

(c)

(d)

(a)

(b)
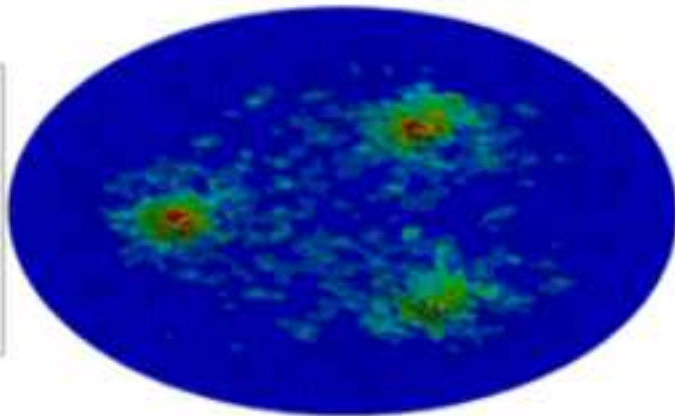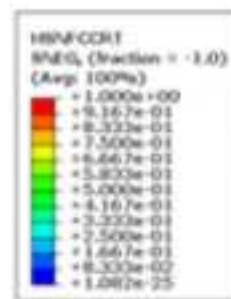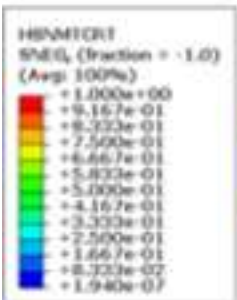
Figure 26
Click here to download high resolution image

S, Mises
(Avg: 100%)
+7.098e-01
+6.507e-01
+5.915e-01
+5.324e-01
+4.733e-01
+4.141e-01
+3.550e-01
+2.959e-01
+2.367e-01
+1.776e-01
+1.185e-01
+5.932e-02
+1.882e-04